الجمهورية الجزائرية الديمقراطية الشعبية

The People's Democratic Republic of Algeria

وزارة التعليم العالي و البحث العلمي

جامعة الشهيد حمة لخضر –الوادي

University of Echahid Hamma Lakhdar –EL OUED

**Faculty of Exact Sciences** — **كلية العلوم الدقيقة**

**Department of Physics** — **قسم الفيزياء**


**Ref : ………** — **المرجع: ……….**

**Thesis presented for the purpose of obtaining the degree of Doctorate LMD**

**Specialty: Physics**

**Option: Applied Physics**

**SUBJECT OF THE THESIS:**

# Experimental investigation of the performance of the solar still filled with a hybrid nanofluid


Presented by :

**Mr. Abdelkader Bellila**


Soutenue: 25/01/2023

The Member of Jury :

| | | | |
|---|---|---|---|
| **Mr : Fethi Bouras** | **Professor** | **University of El-Oued** | **President** |
| **Mr : Mohammed El Hadi Attia** | **Professor** | **University of El-Oued** | **Supervisor** |
| **Mr : Ahmed Kadhim Hussein** | **Professor** | **University of Babylon, IRAQ** | **Co-Superviso** |
| **Mr : Hocine Ben Moussa** | **Professor** | **University of Batna** | **Examiner** |
| **Mr : Djamel Bechki** | **Professor** | **University of Ouargla** | **Examiner** |
| **Mr : Mohammed Ali Haj Ammar** | **MCA** | **University of El-Oued** | **Examiner** |

**Academic year: 2022/2023**

# *Acknowledgements*

***Firstly,*** *I thank God who lights us the right way*

***Secondly,*** *I wish to express my deep gratitude and my sincere thanks to my supervisor Prof.* ***Mohammed El Hadi Attia*** *for his continuous support, guidance and valuable suggestions during my PhD studies. Many thanks for your constant help, encouragement and sympathetic attitude during times of distress. I am grateful for providing an opportunity to work with you and sincerely appreciate your patience and motivation.*

*Thirdly, I would like to express my sincere gratitude to co-supervisor*

*Prof**. Ahmed Kadhim Hussein***

***I*** *address my thanks to Prof.* ***Fethi Bouras****, Prof.* ***Hocine Ben Moussa****, Prof.* ***Djamel Bechki*** *and Dr.* ***Mohammed Ali Haj Ammar*** *for their acceptance to judge this modest work.*

***Abdelkader Bellila***

# *Dedication*

I dedicate this thesis

To my parents

To my dear wife

To the eyes of my

To my sisters and brothers

To my friends

To those who love me

Thank you all.

**Abdelkader *Bellila***

# contents

# List of figures

# List of figures

# List of tables

# List Of Symbols

| Symbols | Nomenclature | Unit |
|---|---|---|
| $A_s$ | Basin Area with Fins | ($m^2$) |
| $A_g$ | Condensing Cover Area | ($m^2$) |
| $C_p$ | Specific Heat Capacity | (J/kg k) |
| $E_x$ | Exergy Flow Rate | (kJ/ s) |
| $h$ | Heat Transfer Coefficient | ($w/m^2$ k) |
| $h_{fg}$ | Latent Heat of Water Vapor | (J/kg) |
| $I(t)$ | The Intensity of Sun Radiation | ($W/m^2$) |
| $m_{ew}$ | Hourly Water Yield | ($kg/m^2$ h) |
| $P_w$ | Partial Vapor Pressure on The Surface Of Water | ($N/m^2$) |
| $P_{gi}$ | Partial Vapor Pressure at The Inside Gal | ($N/m^2$) |
| $Q$ | Heat Transfer Rate | (W) |
| $T$ | Temperature | ($^{\circ}$C) |
| $v$ | The Velocity of Wind | (m/s) |
| **Greeks** | | |
| $\alpha$ | Absorptivity | |
| $\varepsilon$ | Emissivity | |
| $\varepsilon eff$ | Effective Remittance | |
| $\sigma$ | Stefan Boltzmann Constant | |
| $\tau$ | Transmittance | |
| $\eta$ | Efficiency | |
| $\eta_{daily}$ | The Daily Efficiency | |
| $\psi$ | Petela Function | |
| $\Delta$ | Difference | |
| $\sum$ | Algebraic Sum | |
| $\Sigma\dot{m}_d$ | Accumulative Yield | |
| **Subscripts** | | |
| $a$ | Ambient | |
| $c$ | Convection | |
| $e$ | Evaporative | |
| $gi$ | Glass Inside Surface | |
| $go$ | Glass Outside Surface | |
| th | Thermal | |

| | |
|---|---|
| $ins$ | Insulation |
| $r$ | Radiation |
| $Sky$ | Sky |
| sun | Sun |
| loss | Loss |
| $t$ | Total |
| $b - a$ | Still Basin to the Atmosphere |
| $b - w$ | Still Basin to Saline Water |
| $g - a$ | Glass Cover to the Atmosphere |
| $w - g$ | Saline Water to the Glass Cover |
| $w - g_i$ | Saline Water to the Glass Inside Cover |
| $g_o - a$ | Glass Outside Cover to the Atmosphere |
| EHTC | Evaporative Heat Transfer Coefficient |
| SS | Solar Still |
| HSS | Hemispherical Solar Still |
| TSS | Tubular Solar Still |
| SSSS | Single-Slope Solar Still |
| CHSS | Conventional Hemispherical Solar Still |
| MHSSN | Modified Hemispherical Solar Still with $Al_2O_3$- Water Nanofluid |
| MHSSNS | Modified Hemispherical Solar Still with $Al_2O_3$- Water Nanofluid and Water Sprinkler |
| Case (A) | Modified Hemispherical Solar Still $Al_2O_3$- Water Nanofluid (0.1%) |
| Case (B) | Modified Hemispherical Solar Still $Al_2O_3$- Water Nanofluid (0.2%) |
| Case (C) | Modified Hemispherical Solar Still $Al_2O_3$- Water Nanofluid (0.3%) |
| Case (A2) | Modified Hemispherical Solar Still $Al_2O_3$- Water Nanofluid (0.1%) and Water Sprinkler (0.008 Kg/S) |
| Case (B2) | Modified Hemispherical Solar Still $Al_2O_3$- Water Nanofluid (0.2%) and Water Sprinkler (0.008 Kg/S) |
| Case (C2) | Modified Hemispherical Solar Still $Al_2O_3$- Water Nanofluid (0.3%) and Water Sprinkler (0.008 Kg/S) |

# General introduction

# 1. Motivation:

Water is essential for survival and is necessary for beings, plants, animals, and people. Providing fresh water has recently become a major challenge due to resources scarcity as a result of demographic growth and environmental pollution caused by industrial waste (Attia et al., **2021**; Patel and Modi, **2020**). Non-potable water (saltwater), on the other hand, is available everywhere. Yet, salt water cannot be directly used because it contains different types of salt.

A drinking water crisis is one of a most prominent challenges facing humanity today, and studies indicate that the scarcity of drinking water will become the crisis of the twenty-first century (Kabeel et al., **2018**; Attia et al., **2021a**). The issue of drinking water is the problem of our times, and humanity is more threatened than ever before (Kabeel and Abdelgaied, **2019**; Kabeel et al., **2016**; Attia et al., **2021b**).

Algeria is considered one of the countries that adopted the technology of desalination of seawater to provide safe drinking water. Since 2005 ten stations were completed with a total capacity of about two million cubic meters per day, and additional five plants are preparing to launch soon. These stations have contributed to ensuring water security for 25% of Algerians (Kabeel et al., **2021**; Ashtiani et al., **2020**; Attia et al., **2021c**) However, isolated areas suffer from a scarcity of drinking water, the alternative that currently imposes itself is to use solar energy, as it is renewable, clean (Kabeel et al., **2017**; Kabeel et al., **2017a**; Attia et al., **2021d**). Solar energy is of great importance in meeting human daily energy needs. These types of energy are free and is characterized by its preservation of the environment, so the exploitation of solar energy has become one of the things that save people from a lot of expenses compared to their use of other energy sources (Attia et al., **2020**; Kabeel and Abdelgaied, **2017b**; Bellila et al., **2021**) .

Scientists and researchers have exploited the phenomenon of evaporation using solar energy in the discovery of a device to obtain safe drinking water called solar distillers, which depend mainly on the solar distillation process (Khechekhouche et al., **2020**; Kabeel et al., **2019a**; Attia et al., **2022a**). In this process, the water is evaporated using solar energy, and then the steam condenses again to obtain safe drinking water (Attia et al., **2020a**; Kabeel et al., **2020**).

Distillation requires energy to heat water, which can be saved from solar energy or any cheap fuel. Solar energy is a clean/ alternative source of fossil fuel, the best energy source, and is environmentally friendly for various applications such as water heating, ocean heating, and thermal energy storage (Kabeel et al., **2017**; Kabeel et al., **2019a**; Kabeel et al., **2019b**; Katekar and Deshmukh, **2020**; Attia et al., **2022b**).

Solar distillation is one of the simple methods that provide safe drinking water from salty water (Khechekhouche et al., **2020a**; Attia et al., **2020a**; Attia et al., **2022c**). This method is inexpensive, is simple, and requires solar energy, and a simple device to produce freshwater. Scientists and researchers are constantly looking for various ways to improve the performance of solar stills, such as increasing distillate output, increasing surface area, using energy storage materials, and different designs (Manokar et al., **2020**). The latter has become among the methods adopted for desalination of salt water, and it is the only alternative and the only savior for the world in the near future. Many studies have been conducted using solar radiation to desalinate water (Kabeel and Abdelgaied, **2017b**; Attia et al., **2022c**). There are many methods and devices for water desalination in the world, and the main concern of researchers remains, which is how to enhance a yield of distillation. The following are some advanced research works and efforts to improve the performance of solar distillates.

## 2. Bibliographic study:

Many researchers studied different modifications in solar still and aimed to improve the thermal performance and yield of solar stills using several techniques, which includes the use of energy storage materials, heating water in solar still basins, and use of external collectors.

In this section, various designs of solar still developed include the following: single slope, double slope, inclined, hemispherical, triangular, tubular solar still (TSS), (PV/T) active, “V” type solar still, and pyramid type solar still, which has been discussed. (Tiwari and Kumar, **1988**) studied the performance of the TSS during night-time production based on the effect of brine flow. The daily yield from the TSS was higher than that from the CSS. (Kumar et al., **2008**) analyzed the performance of a “V” type solar still with a charcoal absorber. The overall efficiency was found to be 30.05 and 14.10% for the “V” type solar still with and without the charcoal absorber, respectively. (Kabeel, **2009**) made a pyramidal solar still and used the surface of the concave wick to evaporate, while the four sides of the pyramid remain used for condensation. The results gave the daily production of 4.1 L/m$^2$, the maximum system efficiency is 45%, and the average daily efficiency is 30%, due to the concave surface wick increases evaporation due to the capillary effect. (Dev and Tiwari, **2009**) conducted a theoretical and experimental study of an SSSS device under climatic conditions in Delhi, India. In these conditions, the daily output was about 9.005 kg/m$^2$day for an absorption area of 1 m$^2$. The numerical results are consistent with the founded experimental results. (Kumar and Tiwari, **2010**) studied the performance of a hybrid photovoltaic/thermal (PV/T) active solar still and SSSS. In order to recycle the water through the collectors and transfer them to the solar still, a solar-powered water pump is used between the collector of the solar still and the integrated photovoltaic (PV). The results showed that the maximum daily productivity was 2.26 kg for passive solar still and 7.22 kg for hybrid active solar still, at a water depth of 0.05 m. The experimental study confirmed that active hybrid solar still provides approximately 20% higher efficiency than the SSSS. (Murugavel et al., **2010**) developed a double-slope solar still, tested with a layer of water and various reasonable temperature storage materials. They focused on the study in order to find the best material for storing heat to increase yield, and the researchers concluded that quartzite rocks are the active substance. (Murugavel and Srithar, **2011**) made double-slope solar still. Experimental results showed that maximum productivity was obtained using a surface heating effect (aluminum panels are covered with jute and light black cotton fabrics). (Taamneh and Taamneh, **2012**) designed and fabricated a pyramidal solar still (0.95 m$^2$) and covered with a pyramid-shaped glass cover. It turns out that daily productivity was 2.99 and 2.485 L/day with and without a fan, respectively. (Ahsan et al., **2012**) proposed a TSS with vinyl chloride sheet used as the cover material and polythene film as the cover. It can be inferred that the TSS performance was higher than that of the SSSS. (Arunkumar et al., **2012**; Arunkumar et al., **2012a**) developed hemispherical solar still with an area of (0.7 m$^2$) and a height of 0.10 m, made of 3-mm-thick acrylic sheets made of 4-mm-thick wood with dimensions of 1.10 m × 1.10 m × 0.25 m. Sink sides are insulated with glass wool. (Kabeel et al., **2014**) experimentally studied the effect of external heat exchanger and addition of $Al_2O_3$ nanofluids on a yield level of solar distillation. Inclusion of an external heat exchanger improves productivity by 53.2%. The throughput improves upon the combined effect of the condenser in solar energy and $Al_2O_3$ nanofluids by 116%. (Kabeel et al., **2014a**) experimentally examined the influence of fan and addition of 0.2% of $Al_2O_3$ nanofluids on a yield level of single slope solar still (SSSS). The use of $Al_2O_3$ nanoparticles without operating the fan improves productivity by 89%. increased the amount of the productivity by125% at the combined effect of the running fan and $Al_2O_3$ nanofluids. (Suneesh et al., **2014**) studied of the effect a cotton gauze top cover cooling (CGTCC) in "V" type solar still without and with airflow over the glass cover. The daily yield of the production of "V" type solar still without CGTCC is 3300 mL/$m^2$/day, and production with CGTCC is 4300 mL/$m^2$/day, and production with CGTCC and airflow is 4600 mL/$m^2$/day. (Chaichan and Kazem, **2015**) investigated concentrating solar heater with paraffin wax PCM for its application in improving solar distillation. The authors note that when using paraffin and concentrating solar heater the system concentration efficiency increased by 64.07%, while the heating efficiency increased by about 112.87%, and the system productivity increased by 307.54%. (Hansen et al., **2015**) studied the performance of inclined solar still using different wick materials on different absorber plate configurations. The experimental results showed the maximum daily productivity is 4.28 L/day when using a gradient mesh absorbent board with aqueous coral wool. (Somanchi et al., **2015**) studied the impact of $TiO_2$ nanoparticles and PCM on single basin distiller performance. (El-Agouz et al., **2015**) studied theoretically the performance of inclined solar still with and without water close loop. The researchers concluded that daily yields improved by 57.2% when makeup water was superior compared to CSS. (Omara et al., **2015**) studied the behavior of a solar distiller with CuO nanoparticles and corrugated wick. The authors observed improve of 180% in the yield when utilizing CuO nanoparticles and corrugated wick compared to traditional solar distiller. (Chaichan et al., **2016**) used paraffin wax and they were placed in cylindrical tubes installed at the bottom of the basin, to heat the saltwater. The researchers concluded that adding PCM led to an increase in concentration efficiency and heating system efficiency and increased system productivity by about 50.47, 157.8, and 783%, respectively. (Gupta et al., **2016**) conducted the impacts of CuO nanoparticles and nano-coated walls by different water depth (5 and 10 cm) in a SSSS. They found that the yield for utilizing CuO nanoparticles reached 3.5 and 3.1 L/m$^2$/day at water depth of 5 and 10 cm. (Kabeel et al., **2017a**) investigated a pilot study on solar distiller utilizing CuO, $Al_2O_3$ and heat exchanger. They found that daily productivity improved by about 73.80 and 84.20% when using the $Al_2O_3$ and CuO nanofluids with an integral external capacitor, respectively (Shanmugan et al., **2018**) conducted the behavior of solar distiller with combining $Al_2O_3$ nanofluids, PCM and wick materials. The solar distiller yields due to associated $Al_2O_3$ nanofluids with and without PCM and wick materials is 7.5 and 4.2 kg/m$^2$/day. (Modi and Shukla, **2018**) conducted experimental investigations on volume concentration 0.1% of ZnO nanoparticles on solar still productivity. They found that average thermal efficiency is equal, respectively, to 26.19, 25.39 and 16.74% for three days. (Chaichan and Kazem, **2018**) studied mixing nano- $Al_2O_3$ with paraffin wax to increase the yield of simple solar distillates. Therefore, three solar distillates were made, the first was without any modification, the second contained paraffin wax, and the third was a mixture of nano- $Al_2O_3$ and paraffin wax. The experimental results showed that an increase in the productivity of the solar distillation device was 10.38% when using paraffin wax, and it reached 60.53% when using a mixture of nano- $Al_2O_3$ and paraffin wax compared to the simple distillation crop without any modification. (Nazaria et al., **2019**) $Cu_2O$ studied the impact of and thermoelectric channel on solar distiller performance. The outcomes showed that the stills with CuO and thermoelectric channel found 81% advance in productivity. (Subhedar, **2020**) studied of impact of the $Al_2O_3$ nanoparticles by different volume concentration 0.05 and 0.1% in a solar still. The researchers found that a 0.1% $Al_2O_3$ nanoparticle volume concentration productive gives an increase in productivity compared to that of 0.05% $Al_2O_3$ nanoparticles. (Sharshira et al**., 2020**) studied the effect of the hung pad made up of cotton Filled up by 150 g/m$^2$ of nanoparticles ($Fe_3O_4$ and CuO) to increase productivity. The results showed that adding the hung pad made up of cotton to the basin the increases the yield by around and 42 and 57% for $Fe_3O_4$ and CuO, respectively, compared to the conventional method. (Attia et al., **2020a**) addressed the problem of scarcity of drinking water in winter in the Algerian Sahara. To solve this problem, the experimental setup was modified by adding CuO nanoparticles in the winter to compensate for the weak solar radiation and then comparing the productivity and energy efficiency in the winter and summer seasons. The experimental results showed that the daily exergy efficiency of the conventional solar still in summer and winter is equal to 1.2 and 1.58%, respectively. The use of CuO nanoparticles in winter season has exergy efficiency equal to 2.41%. The daily exergy efficiency of the solar still was increased by 52.5% when using CuO nanoparticles in the winter season. (Kabeel et al., **2017**; Kabeel et al., **2019a**; Kabeel et al., **2019b**; Kabeel et al., **2020**) conducted several experiments on tubular solar still with several techniques to increase daily accumulation.

## 3. Objectives of the thesis:

From the literature, it has been observed that many researchers have used different techniques to increase the productivity of conventional solar still. (Arunkumar et al., **2012a**) reported a comparative study of fresh water produced from pyramid and hemispherical solar stills. Modelling and experimental studies on hemispherical solar still were reported by (Jayaprakash et al., **2012**). However, only a few research works were reported on thermal performances of hemispherical solar still. Similarly, literatures revealed that there was no work reported on hemispherical solar still with exergy analysis.

To achieve this idea. The first part, this thesis mainly focuses on the comparative energy, exergy, efficiency, and condensed fresh water from hemispherical and single-slope solar stills. Furthermore, a comparison of the exergy efficiency using hemispherical cover (hemispherical solar still) and the conventional flat cover (single slope solar still) is analytically analyzed using experimental results. The productivity of solar distillation is compared to each device after subjecting them to the same climatic conditions, on May 25; 2020 and June 3; 2020, for a period of 11 hours between 7 AM and 6 PM.

Second part, two modifications were done on the hemispherical distiller, namely (i) use $Al_2O_3$ nanoparticles with different concentrations (0.1, 0.2 and 0.3%) to increase the evaporation rate, (ii) use of glass cover cooling technology by the water sprinkler to increase the condensation rate a constant rate of 0.008 kg/s. To investigate the influences of $Al_2O_3$- water nanofluid and the glass cover cooling technology by water sprinkler on hemispherical solar distiller performance, three hemispherical solar distillers were designed, constructed, and tested at the same climate conditions. The first is the conventional hemispherical distiller which represents the reference case, the second is the modified hemispherical distiller with $Al_2O_3$-water nanofluid, and the third is the modified hemispherical solar distiller with $Al_2O_3$-water nanofluid and the water sprinkler. These experiments were conducted in the south-eastern regions of Algeria (the city of El Oued) in September 26, 27 and 28; 2020, for a period of 10 hours between 8 AM and 6 PM hours.

## 4. Content of the thesis:

The thesis consists of four main chapters, preceded by a general introduction, as well as two appendices: in the first chapter, the various basic concepts needed to understand the methods of heat transfer with mass transfer, the principle of operation of solar stills, calculations energy and exergy. Offer a bibliographic search for the different types of distillates, it is the topic of the second chapter. The third chapter is devoted to the experimental study of comparing two types of solar stills (hemispherical and single slope).

In the fourth chapter, we presented the experimental results of effect $Al_2O_3$-water-based nanofluid and cooling the glass cover on hemispherical solar still productivity in the form of graphs with explanations. These four chapters are supplemented by a general conclusion, bibliographical references and perspectives, appendix A: Error analysis and appendix B: Experimental results.

# Chaptre 01 :
# Mathematical modeling

## 1.1. Introduction:

The equations used for predicting the energy and exergy performances of a solar still are described in this chapter. In addition, the assumptions made in thermodynamic analysis of solar still are listed. The energy conversion efficiency in solar still was quantified based on first law of thermodynamics. The exergy performance based on the second law of thermodynamics was evaluated to quantify the losses in solar still under different climatic conditions.

## 1.2. Energy analysis:

Depends upon thermodynamics' I$^{st}$ law, energy analysis is conducted to examine and explain the solar system components' thermal behaviours. The equations of energy balance for SS components (basin, brackish water and transparent condensing glass) are as follows**.**

### 1.2.1. Equations of energy balance for basin liner:

The basin liner of sun-absorbed radiation is equivalent to the addition of energy derived from the basin liner, convective heat transfer from the basin liner to saline water and losses on the side of the basin. This equation is expressed as **(**Zurigat and Abu-arabi, **2004).**

$$I(t)A_s \propto_b = m_b c_{pb}[dT_b/dt] + Q_{c,b-w} + Q_{loss} \tag{1.1}$$

$\propto_b$ is the still basin absorptivity is considered as 0.95 (Layek, **2018**).

$Q_{c,b-w}$ is a convective mode of heat transfer from still basin to water can be expressed as **(**Zurigat and Abu-arabi, **2004).**

$$Q_{c,b-w} = h_{c,b-w} A_s (T_b - T_W) \tag{1.2}$$

where $h_{c,b-w}$ is the coefficient of convective heat transfer between basin and water is considered as 135 $W/m^2$ k (Layek**, 2018**).

Heat transfer loss from basin liner to the surrounding atmosphere can be written as (Zurigat and Abu-arabi**, 2004**):

$$Q_{loss} = U_b A_s (T_b - T_a) \tag{1.3}$$

where $U_b$ =14 W/m$^2$k (Layek, **2018**).

### 1.2.2. Saline water-energy balance equation:

The saltwater absorbed energy from the sun, and the absorber plate is equivalent to the addition of the water's heat energy. Heat transfer occurred from saltwater to the inside surface of glazing by three types of heat transfers convection, radiation and evaporation. This can be expressed as,

$$I(t) \propto_w A_s + Q_{c,b-w} = m_w c_{p,w}[dT_w/dt] + Q_{c,w-gi} + Q_{r,w-gi} + Q_{e,w-gi} \quad (1.4)$$

$\propto_w$ is the absorptivity of the brackish water is considered as 0.05 (Layek, **2018**).

$Q_{c,w-gi}$ is the heat transfer that occurred through convection from saline water to inside of the glass can be written as (Zurigat and Abu-arabi, **2004**).

$$Q_{c,w-gi} = h_{c,w-gi} A_s (T_w - T_{gi}) \quad (1.5)$$

where $h_{c,w-gi}$ is the coefficient of convection heat transfer between saline water and inside of the condensing cover can be expressed as (Shukla and Sorayan, **2005).**

$$h_{c,w-gi} = 0.884 \left\{ (T_w - T_{gi}) + \frac{[P_w - P_{gi}][T_w + 273]}{[268900 - P_w]} \right\}^{1/3} \quad (1.6)$$

where

$$P_w = exp\left[25.317 - \frac{5144}{T_w + 273}\right] \quad (1.7)$$

$$P_{gi} = exp\left[25.317 - \frac{5144}{T_{gi} + 273}\right] \quad (1.8)$$

Heat transfer through radiation from water to inside area condensing cover is written by (Zurigat and Abu-arabi, **2004).**

$$Q_{r,w-gi} = h_{r,w-gi} A_s (T_w - T_{gi}) \quad (1.9)$$

$h_{r,w-gi}$ is the coefficient of radiation heat transfer between basin to the inside area of glass can be written as (Zurigat and Abu-arabi, **2004**).

$$h_{r,w-gi} = \varepsilon_{eff} \sigma \left[(T_w + 273)^2 + (T_{gi} + 273)^2\right] (T_w + T_{gi} + 546) \quad (1.10)$$

where

$$\varepsilon_{eff} = \left( {}^{1}/_{\varepsilon_w} + {}^{1}/_{\varepsilon_{gi}} \right)^{-1} \quad (1.11)$$

Heat transfer through evaporation from water to the inside of the glass is expressed by:

$$Q_{e,w-gi} = h_{e,w-gi} A_s \left(T_w - T_{gi}\right) \tag{1.12}$$

$h_{e,w-gi}$ is the coefficient of evaporation heat transfer between water to the inside of condensing cover is written as (Zurigat and Abu-arabi, **2004**).

$$h_{e,w-gi} = [16.273 \times 10^{-3}] \times h_{c,w-gi} \times \left[\frac{P_w - P_{gi}}{T_w - T_{gi}}\right] \tag{1.13}$$

The total heat transfer rate of water to the inside of the condensing cover can be expressed as (Sharshir et al., **2017**).

$$Q_{T,w-gi} = Q_{c,w-gi} + Q_{r,w-gi} + Q_{e,w-gi} \tag{1.14}$$

The total heat loss coefficient between water to the inside of condensing cover can be determined by the following relation (Sharshir et al., **2017**):

$$h_{T,w-gi} = h_{c,w-gi} + h_{r,w-gi} + h_{e,w-gi} \tag{1.15}$$

### 1.2.3. Equations of energy balance for condensing glass:

The condensing glass absorbed energy from the sun and water to the inside of the condensing cover by convection, radiation, and evaporation; heat transfer is equivalent to the combination of heat transfer that occurred via convection and radiation from outside of the glass ambient heat energy received.

$$I(t)\,\alpha_g A_g + Q_{c,w-gi} + Q_{r,w-gi} + Q_{e,w-gi} = Q_{c,go-a} + Q_{r,go-a} + m_g C_{p,g} \left({}^{dT_g}/_{dt}\right) \tag{1.16}$$

$\alpha_g$ is glass material absorptivity is taken as 0.05 (Layek, **2018**).

Heat transfer through convection from outside of the glass to ambient can be expressed as (Sharshir et al., **2017**).

$$Q_{c,go-a} = h_{c,go-a} A_g \left(T_{go} - T_a\right) \tag{1.17}$$

$h_{c,go-a}$ is the coefficient of convection heat transfer between the surface of the condensing cover to ambient can be written in terms of wind velocity(v) as (Sharshir et al., **2017**).

$$h_{c,go-a} = 2.8 + (3.0 + v) \tag{1.18}$$

Heat transfer through radiation from the outside of the condensing glass to the ambient is given as (Zurigat and Abu-arabi, **2004**).

$$Q_{r,go-a} = h_{r,go-a} A_g \left(T_{go} - T_a\right) \quad (1.19)$$

$h_{r,go-a}$ is the coefficient of radiation heat transfer between the outside of condensing cover to atmosphere can be determined by employing following mathematical equation (Shukla and Sorayan, **2005**).

$$h_{r,go-a} = \varepsilon_g \sigma \left[\left(T_{go} + 273\right)^4 - \left(T_{sky} + 273\right)^4\right] / \left(T_{go} - T_a\right) \quad (1.20)$$

$\varepsilon_g$ is the emissivity of glass material is taken as 0.88 (Layek, **2018**).

$\sigma$ is Stefan Boltzmann coefficient, $5.6697 \times 10^{-8}$ W/m$^2$ k$^4$.

where

$$T_{sky} = T_a - 6 \quad (1.21)$$

## 1.3. Energy efficiency:

The energy efficiency of a SS is obtained by the ratio of heat transfer evaporation to the intensity of basin liner absorbed sun energy, which can be expressed as (Dashtban and Tabriz, **2011**).

$$\eta_{th} = \frac{\sum m_{ew} h_{fg}}{\sum I(t) A_s} \times 3600 \quad (1.22)$$

where

$$m_{ew} = \frac{h_{e,w-gi} \times \left(T_w - T_{gi}\right)}{h_{fg}} \times 3600 \quad (1.23)$$

## 1.4. Exergy analysis:

Depends on the II$^{nd}$ law of thermodynamics, exergy analysis calculates the higher amount of work obtained from the energy input. The equations of exergy balance for the SS components (base plate, brackish water and transparent condensing cover) are as follows.

### 1.4.1. Basin liner exergy balance equation:

Falling of solar energy on the basin liner surface can absorb a fraction of exergy

$(\tau_g\tau_w\alpha_b A_s)$ $E_{xsun}$, From this absorbed fraction of exergy, some amount is utilized for heating of saltwater ($E_{x\,c,\,b\text{-}w}$) and a little amount is lost from the insulation ($E_{x\,ins}$) also, the remaining amount is destructed from the basin liner ($E_{x\,des,}$ b) (Layek, **2018**).

$$E_{xdes,b} = (\tau g \tau w \alpha b As) E_{xsun} - \left(E_{xc,b-w} + E_{xins}\right) \quad (1.24)$$

The sun insolation exergy (in W/m$^2$) on the surface of still is given by (Kumar and Tiwari, **2011**):

$$E_{xsun} = I(t) \times A_s \times \Psi \quad (1.25)$$

where $\Psi$ is Petela function can be expressed as:

$$\Psi = \left[1 + \frac{1}{3}\left(\frac{T_a}{T_s}\right)^4 - \frac{4}{3}\left(\frac{T_a}{T_s}\right)\right] \quad (1.26)$$

where

$$E_{xc,b-w} = A_s h_{c,b}(T_b - T_w)\left(1 - \frac{T_a}{T_b}\right) \quad (1.27)$$

$$E_{xins} = A_s h_b (T_b - T_a)\left(1 - \frac{T_a}{T_b}\right) \quad (1.28)$$

## 1.4.2. Saline water exergy balance equation:

The saline water absorbed exergy is the combination of the exergy transferred from the basin to that received via the saline water. Some amount is transferred via three modes of heat transfer between brackish water to inside the glass from this exergy. The remaining amount is destroyed from the saline water ($E_{des,\,w}$).

$$E_{xdes,w} = (\tau_g \alpha_w As) E_{xsun} + E_{xc,b-w} - E_{xt,w-gi} \quad (1.29)$$

$E_{xt,w-gi}$: Total exergy transfer from brackish water to the inner side of condensing glass is given as (Layek, **2018**).

$$E_{xt,w-gi} = E_{xc,w-gi} + E_{xr,w-gi} + E_{xe,w-gi} \quad (1.30)$$

where

$$E_{xc,w-gi} = A_s h_{c,w-gi}(T_w - T_{gi})\left(1 - \frac{T_a}{T_w}\right) \quad (1.31)$$

$$E_{xr,w-gi} = A_s h_{r,w-gi}(T_w - T_{gi})\left[1 + \frac{1}{3}\left(\frac{T_a}{T_w}\right)^4 - \frac{4}{3}\left(\frac{T_a}{T_w}\right)\right] \quad (1.32)$$

$$E_{xe,w-gi} = \mathrm{A}_{S}\mathrm{h}_{e,w-gi}(T_w - T_{gi})\left(1 - \frac{T_a}{T_w}\right) \tag{1.33}$$

### 1.4.3. Transparent glass cover exergy balance equation:

The expression for transparent condensing cover exergy balance is given as (Layek, **2018**).

$$E_{xdes,g} = \alpha_g \mathrm{A}_g I_T \Psi + \mathrm{E}_{xt.w-gi} - E_{xt,go-a} \tag{1.34}$$

where

$$E_{xt,go-a} = \mathrm{E}_{xc.go-a} + E_{xr,go-a} \tag{1.35}$$

$E_{xt,go-a}$ is total exergy transfer from exterior side of condensing cover to the surrounding area is given as (Layek, **2018**).

$$E_{xc,go-a} = A_g \mathrm{h}_{\mathrm{c,go-a}}(T_{go} - T_a)\left(1 - \frac{T_a}{T_{go}}\right) \tag{1.36}$$

$$E_{xr,go-a} = A_g h_{r,go-a}(T_{go} - T_a)\left[1 + \frac{1}{3}\left(\frac{T_a}{T_{go}}\right)^4 - \frac{4}{3}\left(\frac{T_a}{T_{go}}\right)\right] \tag{1.37}$$

## 1.5. Exergy efficiency:

The exergy efficiency of SS is obtained by the ratio of exergy output to exergy input, and is written as (Kumar and Tiwari**, 2011**).

$$\eta_{ex} = \frac{Exergy\ output}{Exergy\ input} = \frac{E_{xoutput}}{E_{xinput}} \tag{1.38}$$

The exergy output (evaporation output) per hour of a solar still system can be defined as (Kumar and Tiwari**, 2011**):

$$E_{xoutput} = E_{evap} = \frac{m_{ew} \times L}{(3600_s . h^{-1})} \times \left(1 - \frac{T_a + 273}{T_w + 273}\right) \tag{1.39}$$

$m_{ew}$ is the hourly output of potable water yield (kg/h).

The exergy input of SS is determined as (Kumar and Tiwari, **2011**):

$$E_{xinput} = E_{xsun} \tag{1.40}$$

## 1.6. Conclusion:

This chapter is helpful to evaluate the thermal analysis of the different hemispherical and single slope solar stills. The equations are written to find the energy and exergy efficiency of the performances of a solar still. The equations of the energy conversion efficiency in solar still was calculated based on first law of thermodynamics. The equations the exergy performance based on the second law of thermodynamics was calculated to quantify the losses in solar still.

# Chaptre 02:

# Different type of solar distillers

## 2.1. Introduction:

One of the huge problems in this world is the lack of drinking water. Algeria is not immune to this problem. Several distillation methods have been adopted, but solar distillation remains the simplest and most economical of all methods. Despite its low efficiency compared with other technologies, it has a great advantage as it uses solar radiation. There are different types of solar stills built in different countries on the world, which in common have a saline water basin with a black bottom, a transparent cover and collecting pipes, which give the condensed water as end product.

In this chapter, we will mention nine types of solar distillates (single slope, double slope, vertical, multiple-effect, spherical, tubular, concave, stepped and hemispherical).

## 2.2. Different type of solar distillers:

There are different types of solar stills built in different countries on the world, which in common have a saline water basin with a black bottom, a transparent cover and collecting pipes, which give the condensed water as end product. Sunlight heats the water in the basin. This heated water evaporates and recondenses on the underside of transparent cover and runs down into collecting through along the inside lower edges of the transparent cover.

### 2.2.1. Single slope solar still:

Figure (2.1) shows the schematic and experimental diagram of single slope solar still. Single slope solar still sink is made of a wooden box with a square base area of example (0.25, 0.5 and 1 $m^2$). The lid is inclined at an angle of according to the location of the experiment region from the horizon. For better absorption of solar energy, the inner surfaces are coated with black silicone. Also, (3, 4 and 5 mm) thick glass is used to cover the solar cover (Attia et al., 2021; Khechekhouche et al., 2019).

In the solar box, water is added manually or automatically by a float system. Solar energy, passing through the top glass of the box, heats the water to its point of evaporation. The water vapor produced condenses on the relatively cooler glass. This, on a slight slope, leads the distilled water to a storage container.

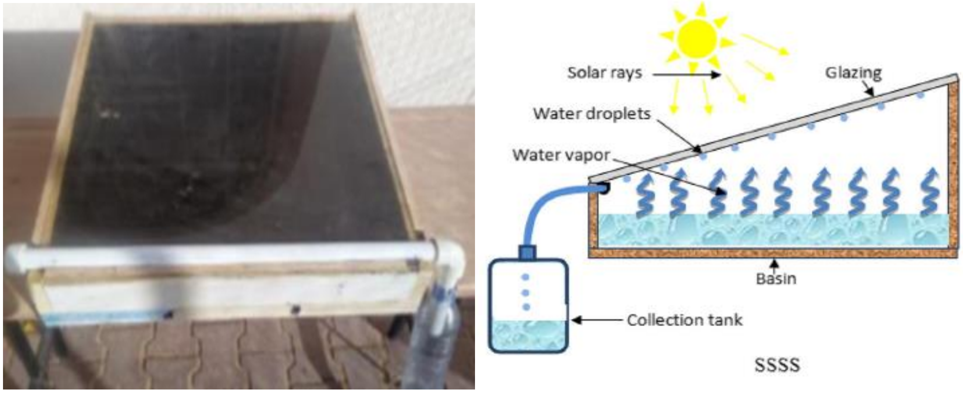


**Figure (2.1):**Schematic and experimental representation of single slope solar still (Attia et al., **2021**).

### 2.2.2. Double sloped solar still:

Figure (2.2) shows the schematic and experimental solar still with a triangle shaped glass. The glass is attached to the basin and two distillation pipes collect the condensed water, on each side of the rectangular glass to the bucket. The basin is usually made of a good insulator of heat and painted black to avoid heat losses. An absorber plate is usually used which is black in color to absorb all incident radiations to the still (Murugavel et al., **2008**).

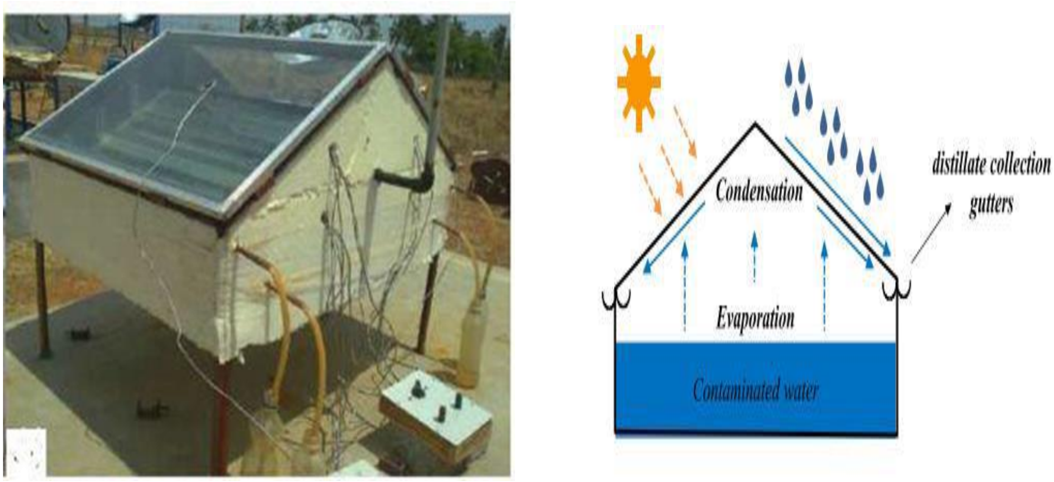


**Figure(2.2):** Schematic and experimental representation of double slope solar still (Murugavel et al., **2008**).

### 2.2.3. Vertical solar still:

Figure (2.3) present a vertical solar still, taking into consideration the development of a highly productive solar still which is simple enough to be constructed and maintained by local technicians in the developing countries. The proposed still consists of a flat plate reflector, casters for manual azimuth tracking and a vertical multiple-effect diffusion still, which consists of a glass cover and a series of closely spaced vertical and parallel partitions. Each partition is in contact with a saline-soaked wick. Saline water is continuously fed to the wicks. Direct and diffuse solar radiation, and solar radiation reflected by the flat plate reflector transmit through the glass cover and are absorbed on the front surface of the first partition. The absorbed solar energy is recovered and recycled in the vertical still to increase distillate productivity (Tanaka et al., **2009**).

A schematic diagram and a snapshot of the outdoor experimental apparatus is shown in Figure (2.4). The still consists of a 5-mm-thick glass cover, the first partition (a 1-mm-thick copper plate) and the second to the last partitions (0.5-mm-thick stainless-steel plates). The wet wick (cotton flannel about 0.5 mm thick) was attached to the rear surface of each partition by capillary force. The absorbing area for the sunrays of the front surface of the first partition was about 0.097 $m^2$ (0.294 min height and 0.329 min width). The front surface of the first partition was coated with the selective absorber (Solar Paint, Okitsumo Co., emittance is 0.32 and absorptance for sunrays is 0.92). A-1.8 mm-thick mirror-finished stainless-steel plate (reflectance is 0.7) was used as the flat plate reflector and the area of the reflector was almost the same as the solar absorbing area of the first partition (Tanaka et al., **2009**).

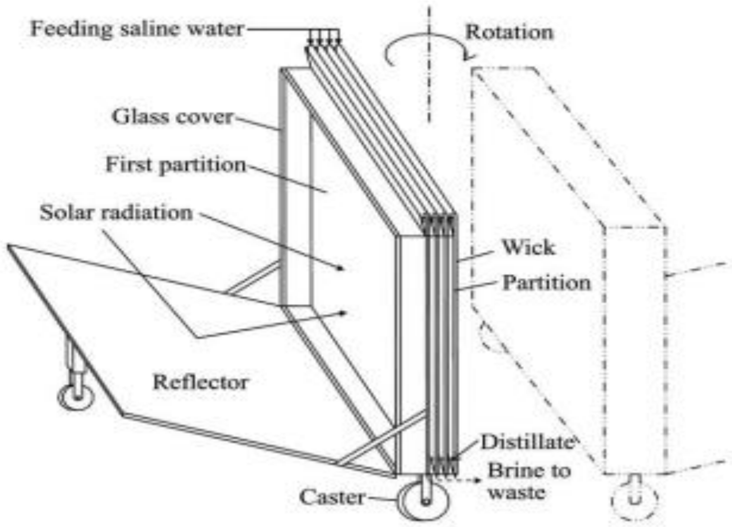


**Figure (2.3):** Schematic diagram of a proposed still (Tanaka et al., **2009**).

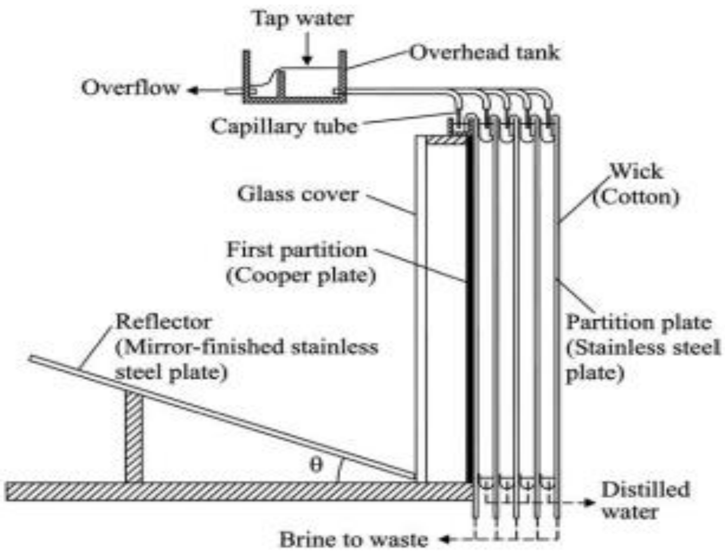


**Figure (2.4):** Schematic diagram of an experimental apparatus (Tanaka et al., **2009**).

### 2.2.4. Multiple-effect solar stills:

Solar stills of various structures have been proposed and examined to determine their productivity and feasibility. Among them, multiple effect stills have greater productivity than conventional single-effect stills such as a basin-type still and a tilted-wick still, since the latent heat of condensation contributes further evaporation of saline water to recover and recycle solar energy in the multiple-effect stills are shown in Figure (2.5) and Figure (2.6). The various types of multiple-effect stills have been studied (Tanaka et al., **2009**). Among the multiple-effect stills, the multiple-effect diffusion still, which consists of a series of closely spaced parallel partitions in contact with saline-soaked wicks, has great potential because of their high productivity and simplicity. Solar energy absorbed on the front surface of the first partition causes evaporation of saline water in the wick attached to the rear surface of the first partition. Water vapor diffuses through the narrow humid air layer between the first and second partitions and condenses on the front surface of the second partition. Latent heat of condensation contributes to further evaporation of saline water in the wick attached to the rear surface of the second partition. In this manner, the evaporation and condensation processes are repeated in the multiple effect diffusion still to increase distillate productivity (Tanaka et al., **2009**).

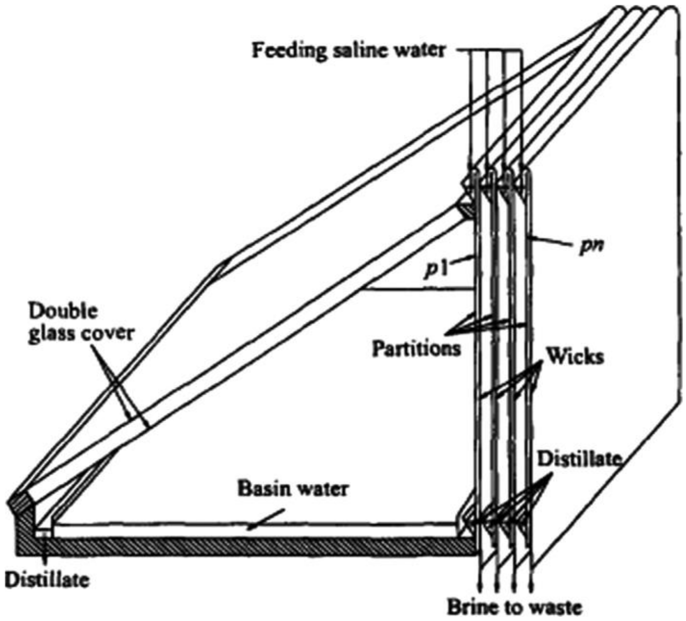


**Figure (2.5):** Multiple-effect basin type diffusion-coupled solar still (Tanaka et al., **2009**).

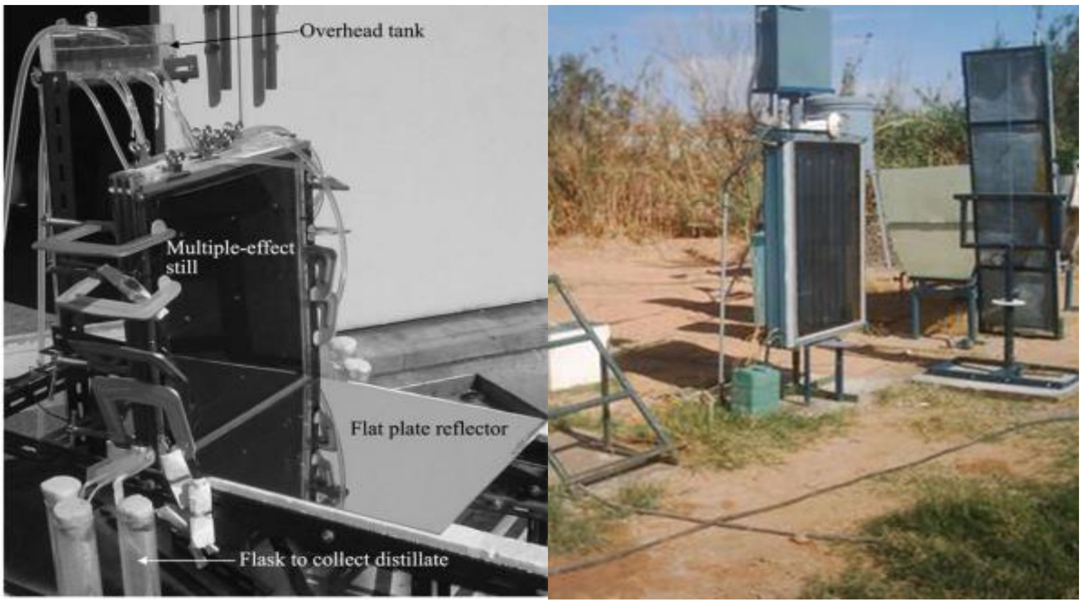


**Figure (2.6):** Photo of an experimental apparatus (Tanaka et al., **2009**).

## 2.2.5. Spherical solar still:

A spherical solar still design with collector area of 0.28 m$^2$ is presented. The still consists of a shallow circular basin of diameter 0.60 m that is made of steel. The circular absorber basin is coated with black paint for maximum absorption of incident solar radiation. The circular basin is fixed at the middle of the spherical aluminum mesh at radial height of 0.28 m. The saline water is stored in a basin with a capacity of 16 liters. The basin in the spherical solar still is fitted without having any physical contact with the top cover made of low-density polyethylene sheet. The low-density polyethylene sheet of thickness 0.107 mm is spread over the spherical mesh. A gap of 0.03 m is maintained between the circular basin and top cover. The evaporated water, which is condensed on the top cover, passes between this gap, and drips down towards the distilled water collection segment as illustrated in Figure (2.7) and Figure (2.8), shows the pictorial diagram of the spherical solar still with total height of about 0.63 m (Arunkumar et al., **2012**).

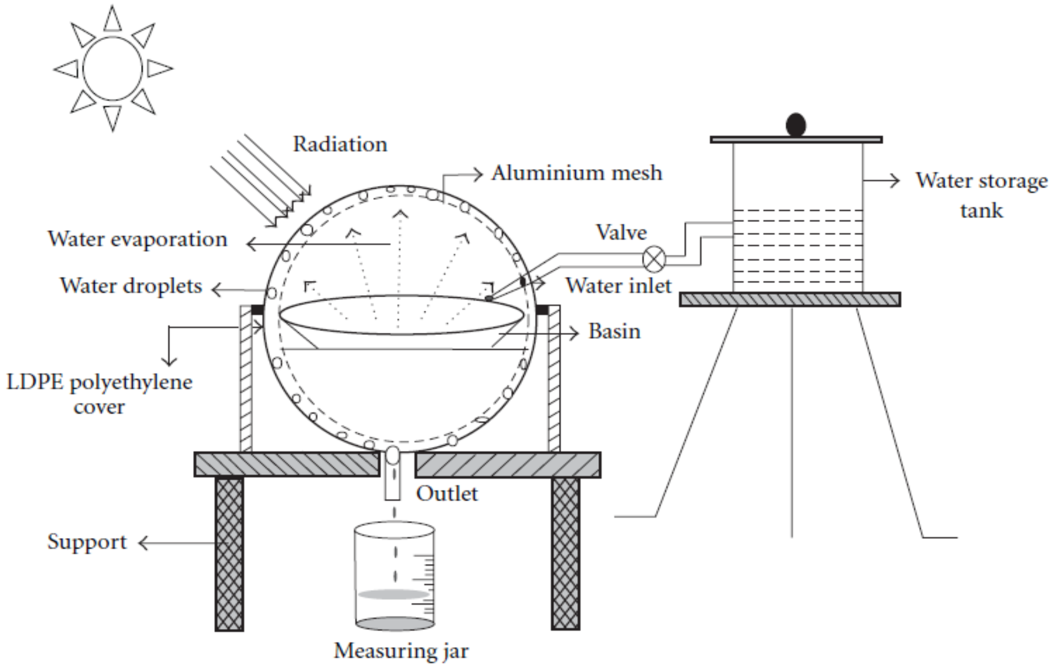


**Figure (2.7):** Schematic diagram of a spherical solar still (Arunkumar et al., **2012**).

**Figure (2.8):** Pictorial view of spherical solar still (Arunkumar et al., **2012**).

### 2.2.6. Tubular solar still:

The tubular solar still consists of a cover made of transparent acrylic transparent tube, steel rectangular water basin and metal support frame, as shown in Figure (2.9) and Figure (2.10). Most of the solar thermal heat, which transfers across the cover is absorbed by the saline water in the basin and the rest is absorbed by the cover and the basin materials. This thermal process makes the salty water heated and evaporates. The water vapor density of the humid air increments associated with the evaporation from the water surface. The lower cover inner surface temperature makes the water vapor condenses when contacts it, releasing its latent heat due to evaporation. The condensed water flows down to the cover bottom by gravity effect due to the inclination of the cover then collected (Elshamy et al., **2018**).

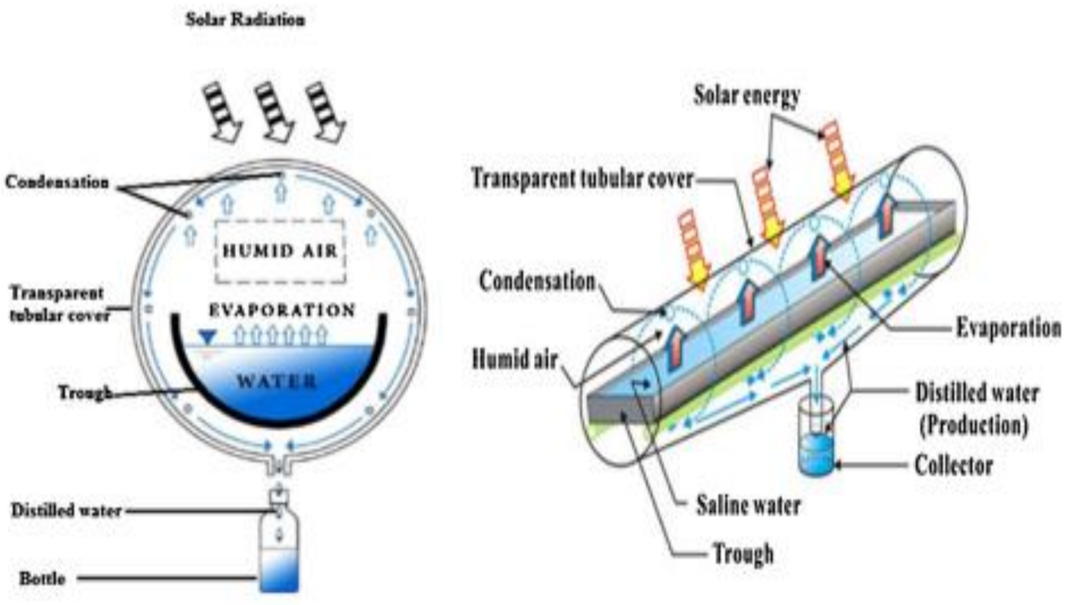


**Figure (2.9):** Tubular solar still model (Elshamy et al., **2018**).

**Figure (2.10):** Photo of tubular solar still model (Elshamy et al., **2018**).

### 2.2.7. Concave solar still:

Concave type solar still is designed and constructed for the purpose of experimental work. Figure (2.11) (a and b) shows a schematic diagram of the solar still and a photograph of this solar still is shown in Figure (2.11) a. The basin of the solar still is concave with a square aperture of 1.2 m × 1.2 m. Its frame is fabricated from steel of 2 mm thickness. The still basin is made of galvanized steel. The bottom and sides of the basin are insulated by glass wool of 5 cm thick layer surrounded by a steel sheet 2 mm thickness. The basin surface is black painted to absorb maximum solar radiation. The basin depth is 30 cm at the center. The depth of saline water in the still is 10 cm at the center. Glass cover is used at four sides of the solar still with ordinary window glass of 3 mm thickness and tilted at an angle of 45 degree to the horizontal surface (Kabeel et al., **2009**). The distillate is collected by a galvanized iron channel fixed on the sides at the lower end of the glass cover and is taken out through two PVC pipes to two graduated flashes as shown in Figure (2.11) b. The channels were inclined such that no accumulation of water was observed. The whole system is made vapor tight using silicone rubber as a sealant to prevent any vapor leakage. One of the four glass cover faces south direction (Kabeel et al., **2009**).

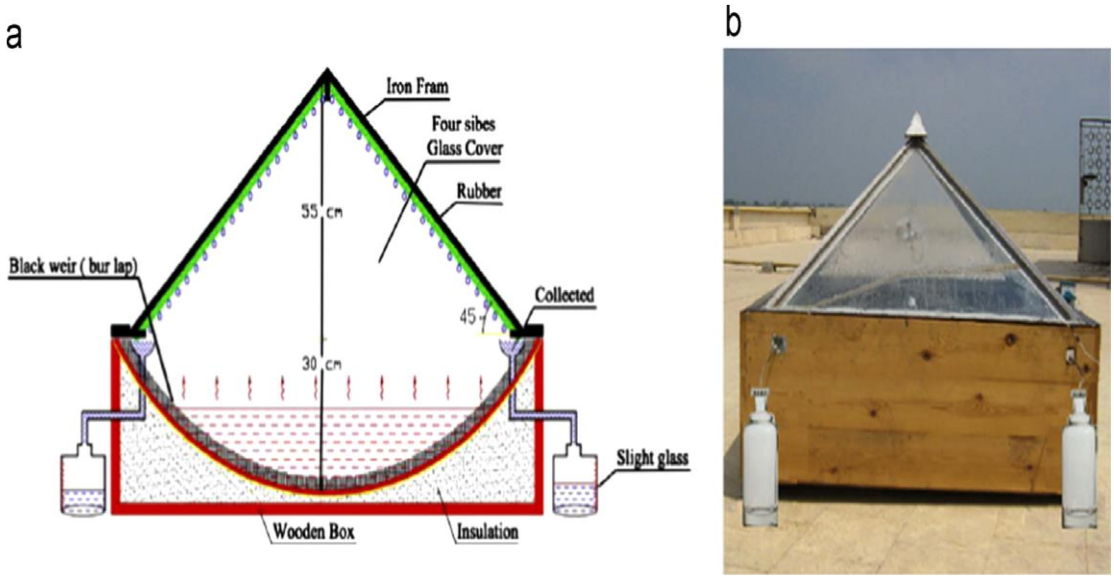


**Figure (2.11):** Concave type solar still: (a) schematic, (b) experimental setup (Kabeel et al., **2009**).

## 2.2.8. Stepped solar still:

Figure (2.12) shows a photo of the erected stepped solar still. In addition, the schematic diagram of the experimental setup is shown in Figure (2.13). It consists of a saline water tank, a vacuum tube solar collector, a conventional still (single basin solar still) and a stepped solar still. Basin area of the conventional still is 1 $m^2$ (0.5 m × 2.0 m). High-side wall depth is 45 cm, and the low-side wall height is 160 mm. The still is made of Galvanized steel sheets. The whole basin surfaces are coated with black paint from inside to increase the absorptivity. Also, the still is insulated from the bottom to the side walls with sawdust of 4 cm thick to reduce the heat loss from the still to ambient. The insulation layer is supported by a wooden frame. The basin is covered with a clear glass sheet (3, 4 and 5 mm) thick inclined at nearly angle horizontally, which is the latitude of experiment region to maximize the amount of incident solar radiation. The whole experimental setup is kept in the south direction to receive maximum solar radiation throughout the year (Kabeel et al., **2012**).


**Figure (2.12):** A photo of the experimental setup (Kabeel et al., **2012**).

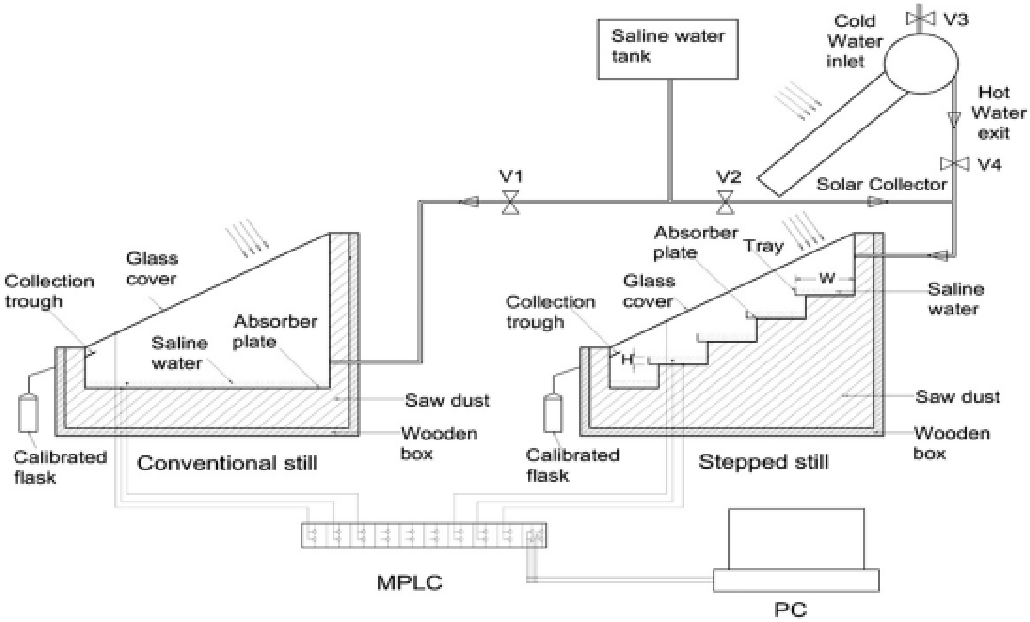


**Figure (2.13):** Schematic diagram of the experimental set up (Kabeel et al., **2012**).

## 2.2.9. Hemispherical solar still:

A schematic diagram of the new hemispherical (dome-shaped) solar still is shown in Figure (2.14). The still mainly consists of the circular basin (tray) and absorber plate carrying the saline water, the hemispherical cover, the conical-shaped distillate collector, the distillate output plastic container, and the mobile support structure (trolley), as shown in Figure (2.14) and Figure (2.15). The basin of the still (tray) and absorber plate, and the collector were all fabricated using aluminum. The basin contains the absorber aluminum plate which has a surface area of 0.5 $m^2$ and a thickness of 4 mm. A hole with diameter of approximately 25.4 mm was drilled into the tray to provide accessibility of saline water into the basin during initial filling and the bottom section of basin was insulated to reduce thermal losses to the surroundings. The absorber was coated with black paint to maximize absorption of the incident solar radiation on the basin (Ismail, **2009**). The hemispherical cover, located on the top of the solar still unit, was made of a transparent plastic with absorptivity and transmissivity equal to 0.9 and 0.8, respectively. The transportable support structure was made of galvanized steel and coated with green paint. For sealing purpose, an approximately 6.5 mm thick rubber ring gasket was used and placed between the cover and the collector support structure where they were tightened and held in place using C-type clamps placed at equal distances around the periphery of the still as shown in Figure (2.14). The distillate output from the still was frequently collected using a plastic container placed under the nozzle outlet part of the conically shaped collector. Copper thermocouples were installed and used to measure the temperature of the water in the basin at several locations to ensure uniform temperature throughout the basin, and the temperatures of the inside cover and ambient (Ismail, **2009**).

**Figure (2.14):** Photographs of the fabricated hemispherical solar still (Ismail, **2009**).

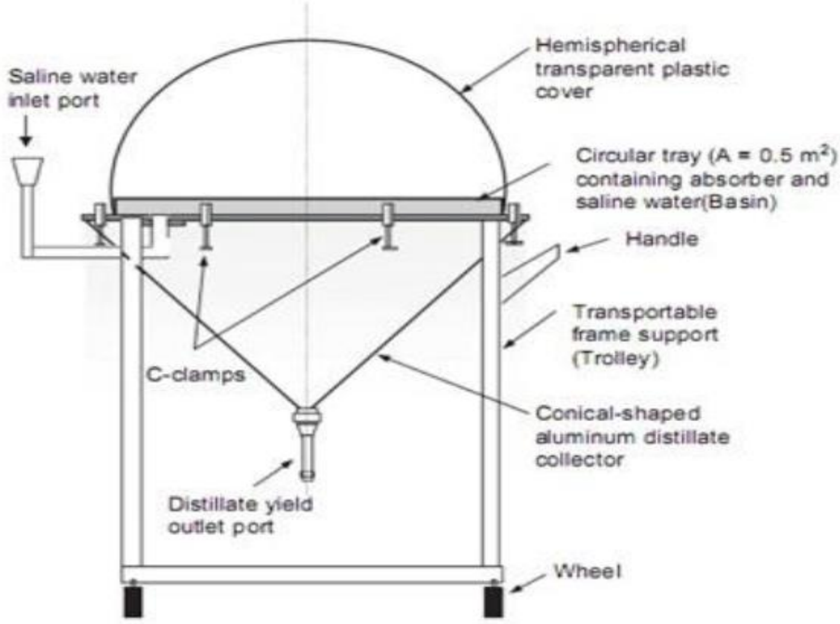


**Figure (2.15):** Schematic diagram of the new transportable hemispherical solar still (Ismail; **2009**).

## 2.3. Conclusion:

Our objective is the establishment of some experiments aimed at measuring the production of distilled water from a solar still installed in the Saharan region of south-eastern Algeria exactly in the region of El-Oued, we have seen in this chapter the different types of solar stills, their operating principles and the influential parameters on a solar still.

We have chosen two types of greenhouses solar still to be the subject of our study in the following chapters. We chose the single-slope and hemispherical solar still. Finally, we classify the parameters that affect the distillation operation from internal and external parameters.

# Chaptre 03:

# A comparative study of hemispherical and single slope solar stills yields.

## 3.1. Introduction:

Solar still is one of the easiest methods that provide safe drinking water from saline water. This method is inexpensive, simple, and requires solar energy, and a simple device to produce freshwater. Researchers are continuously looking for several methods to augment the output of the solar still, such as enlarging surface area, using energy storage materials, and devising different designs.

In this chapter, the daily accumulation of distilled water produced for hemispherical solar still and single-slope solar still was measured. Relative energy and exergy efficiency studies of both distilleries has been carried out is to compare the thermal performance of a hemispherical solar still and single slope solar still using condensed water production, thermal and exergy efficiency are compared, in order to select the optimum still.

## 3.2. Experimental setup steps:

### 3.2.1. Description of the experimental model designs:

The experimental model design is the preliminary task of each and every research. As presented in Figure (3.1), the hemispherical solar still is made with a cylindrical basin having a diameter of 0.38 m, and a depth of 0.04 m made of wood, and the area of the spherical basin is 0.1 $m^2$. The inner surfaces of the basins are coated with black silicon for better absorption of solar energy, and provision is provided to collect the distilled water after condensation. In order to cover the hemispherical solar still, plastic cover with thickness of 3 mm and a diameter of 0.40 m is used to collect the water droplets formed in the inner cover. Figure (3.2) shows the schematic drawing of the hemispherical solar still and single slope solar still. The basin of single slope solar still is made with a wooden box with a square base area of 0.25 $m^2$. The height of the back side is 0.14 m, the height of the front side is 0.06 m, and cover is tilted with angle 10 degrees with the horizon. For enhanced absorption of solar energy, the inner surfaces are coated with black silicon. Also, a glass with a thickness of 3 mm is used to cover the solar still.

**Figure (3.1):** Distilled hemisphere basin.

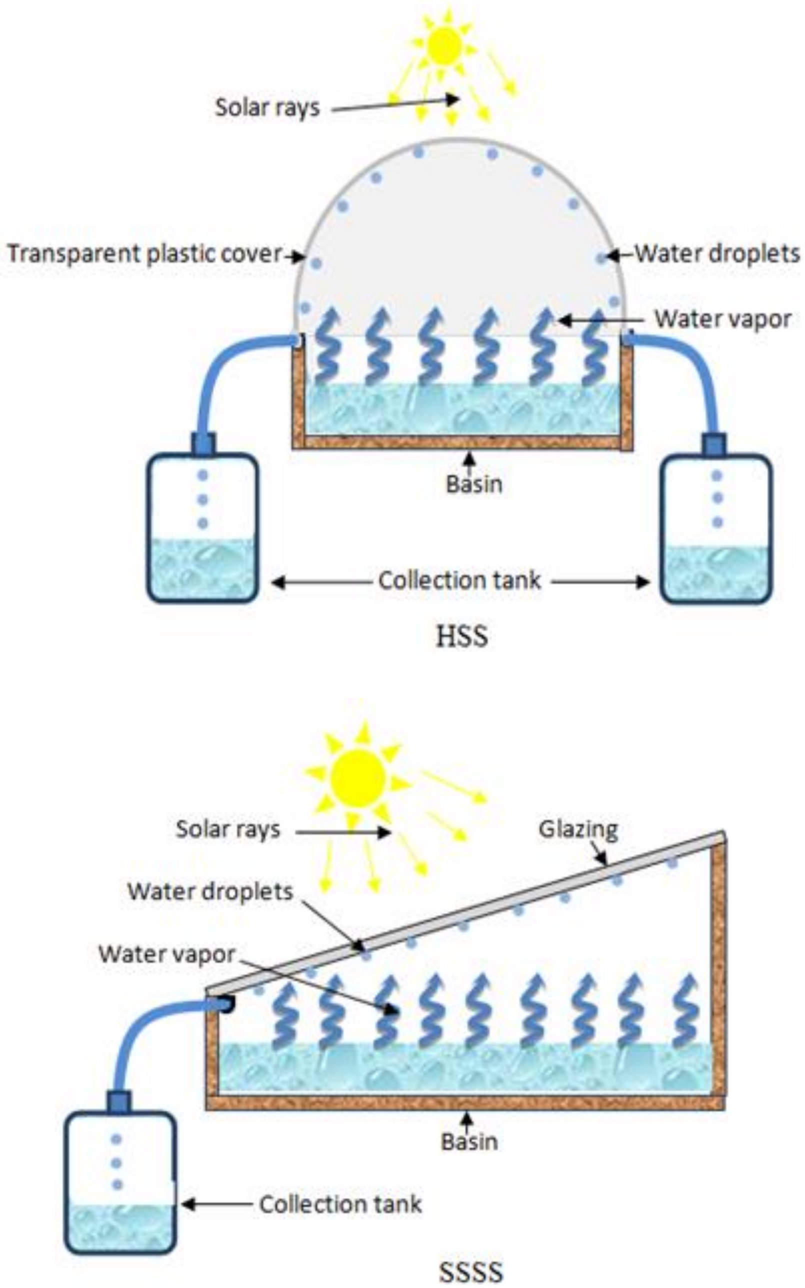


**Figure (3.2):** Schematic representation of the hemispherical solar still and single slope solar still.

## 3.2.2. The climatic conditions:

In order to compare the performance of a solar still using a conventional single slope cover and hemispherical cover. The daily production of palatable water is compared after experimented at the same conditions. The study was carry out in El Oued, Algeria, situated in 6° 47' E and 33° 30' N for a period of 11 hours between 7 and 18 Hrs on May 25, 2020, and June 03, 2020. The climatic conditions during the studies are tabulated in Table (3.1).

**Table (3.1):** The weather conditions for the experimental day.

| Date | May 25, 2020 | June 03, 2020 |
|---|---|---|
| Sunrise | 05:34 AM | 05:25 AM |
| Sunset | 07:25 PM | 07:33 PM |
| Ambient temperature | 21-37 °C | 23-39 °C |
| Humidity | 18-23 % | 16-22 % |
| Wind speed | 20 km/h | 17 km/h |
| Pressure | 102331 Pa | 102325 Pa |

## 3.3. Experimental procedure:

Figure (3.3) shows the experimental photograph of two solar stills. The two stills were tested under the same climatic conditions, and we filled with the same quantity of saltwater its salinity is 3 g/L by maintaining the depth of water as 1 cm constantly. The quantities of water inside hemispherical solar still and single slope solar still are 1 kg and 2.5 kg of saltwater. The duration of the experiment is from 7:00 Hrs and 18:00 Hrs.


**Figure (3.3):** Experimental setup.

## 3.4. Measurements and errors:

Table (3.2) shows the accuracy, range, and the standard uncertainty of the instruments used in the current investigation. Three thermocouples have been fixed in the hemispherical solar still to measure the temperatures of the inner glass, outer glass, and saline water temperature. The thermocouples are attached to the different elements of the solar still to estimate the temperature of basin water, inner and outer cover. The temperature of ambient is also estimated using thermocouple. The solar power meter is used to measure solar radiation for the day of the experiment.

**Table (3.2):** Accuracy, range, and standard uncertainties of measuring devices.

| Instrument | Accuracy | Range | Standard uncertainty |
|---|---|---|---|
| Solar power meter | ± 10 W/m$^2$ | 0-1999 W/m$^2$ | 5.69 W/m$^2$ |
| Thermocouple | ± 0.1 °C | −100–500 °C | 0.05 °C |
| Graduated cylinder | ± 1 ml | 0–250 ml | 0.5 ml |

## 3.5. Result and discussion:

In order to compare single slope solar still and hemispherical solar still, we draw time-wise changes in temperature and radiation profile variation for single slope solar still and hemispherical solar still, time-wise changes of evaporative heat transfer coefficient (EHTC) and condensed water production, time wise changes in energy and exergy efficiency, and comparison of daily productivity of the present study on various still designs.

### 3.5.1. Temperature and radiation profile variation for SSSS and HSS:

Figure (3.4) is plotted for the recorded temperature and solar radiation profile on hourly basis for single slope solar still, hemispherical solar still on 25.05.2020, and 03.06.2020. From Figure (3.4), it is identified that the radiation from the sunrise keeps on increasing and reaching the maximum value at 12:00 Hrs and measured as 1004 and 1008 W/m$^2$ on 25.05.2020 and 03.06.2020 respectively. Also, Ta increased in sunrise hours and measured its uppermost value at 13:00 Hrs (37 °C on 25-5-2020 and 37 °C on 3-6-2020). The daily average in solar radiation on 25.05.2020, and 3.06.2020 is estimated as 661.25 W/m$^2$ and 672.58 W/m$^2$ and the mean temperature of ambient is estimated as 31.33 °C, and 34.50 °C respectively. On hourly basis the solar radiation increases which simultaneously increase the solar still elements such as water, and cover temperature. The basin water temperature in peak solar radiation is measured as 63 and 68 °C on 25.05.2020, while on 03.06.2020 it is observed as 64 and 69 °C using conventional single slope and hemispherical solar still respectively. The water temperature is enhanced to about 7.81% using hemispherical cover than the single slope solar still. The improvement is due to the reduction of shadow effect falling on the absorber surface area using hemispherical cover than the single slope solar still. The average temperature of water during the experimental days using conventional and hemispherical solar still are 50.67 and 51.50 °C on 25.05.2020, while on 3.06.2020 it is found as 53.17 and 54.08 °C respectively.

The temperature of glass measured at peak solar intensity using conventional and hemispherical solar still on 25.05.2020 is recorded as 53 and 54 °C while with an average solar radiation of 672.58 W/m$^2$ the temperature of glass cover is measured as 54 and 55 °C respectively. The increased temperature of glass cover using hemispherical solar still is 1 °C higher than the single slope solar still which is due to the higher rate of evaporation by the water placed in the basin. The average temperature of hemispherical cover and the single slope solar still is estimated as 41.92 °C and 42.33 °C respectively. On increased radiation, the hemispherical cover temperature is higher than the single slope solar still whereas, during the afternoon (reducing solar radiation) the temperature of hemispherical cover is lower than the single slope solar still. It is also found that temperature difference among water and cover is higher in the hemispherical solar still than the single slope solar still.

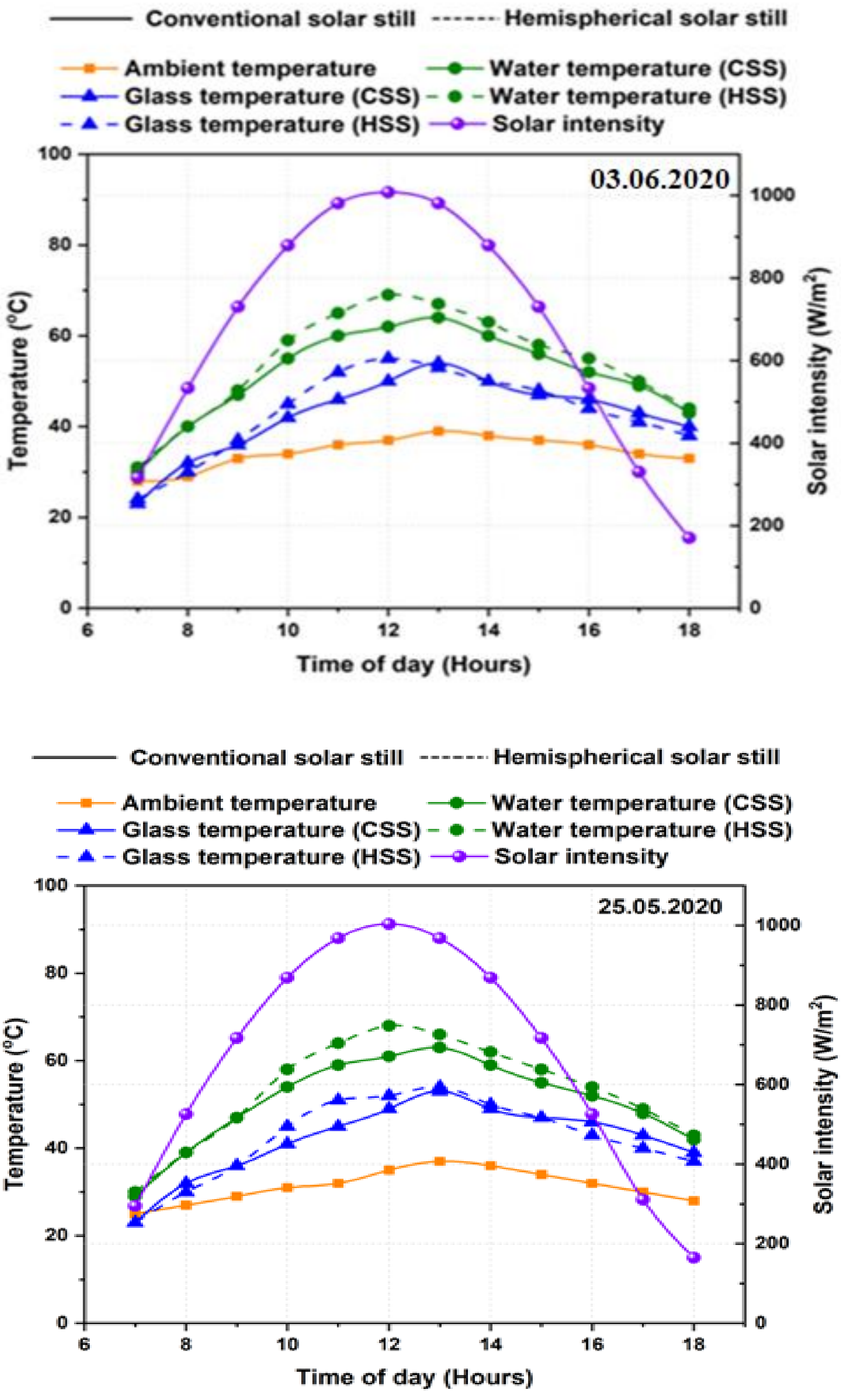


**Figure (3.4):** Temperature and solar radiation profile for single slope solar still and hemispherical solar still, on a 25-5-2020 and b 3-6-2020.

### 3.5.2. Time-wise changes of EHTC and condensed water production:

Figure (3.5) displays the time-wise changes of EHTC and condensed water production from the single slope solar still and hemispherical solar still. The highest calculated EHTC and yield production from the single slope solar still on 25-5-2020 are 26.22 W/m$^2$ and 0.57 kg, and the corresponding EHTC and peak yield on 3.06.2020 is found as 27.69 W/m$^2$ and 0.59 kg, respectively. Likewise, the highest EHTC and condensed water production from the hemispherical solar still on 25-5-2020 is 33.84 W/m$^2$ and 0.92 kg, on 3-6-2020 is 35.10 W/m$^2$ and 0.97 kg, correspondingly. The highest calculated EHTC for the hemispherical solar still is 7.62 W/m$^2$ higher than the single slope solar still on 25-5-2020 and 7.41 W/m$^2$ higher than the single slope solar still on 3-6-2020. The peak condensed water generation from the hemispherical solar still is 0.35 kg higher than the single slope solar still on 25-5-2020 and 0.38 kg higher than the single slope solar still on 3-6-2020. In the hemispherical solar still, the rate of condensed water generation from the briny water is higher than the single slope solar still since it has larger collector cover. The daily average calculated EHTC and total condensed water production from the single slope solar still on 25-5-2020 are 16.22 W/m$^2$ and 3.36 kg, on 3-6-2020 is 17 W/m$^2$ and 3.64 kg, correspondingly. Likewise, daily average EHTC and total condensed water production from the hemispherical solar still on 25-5-2020 is 19.4 W/m$^2$, and 4.9 kg, on 3-6-2020, is 20.3 W/m$^2$ and 5.38 kg, correspondingly. The daily average EHTC of the hemispherical solar still and daily condensed water production from the hemispherical solar still is 3.18 W/m$^2$ and 1.53 kg higher than the single slope solar still on 25-5-2020, and daily average EHTC of the hemispherical solar still and daily condensed water production from the hemispherical solar still is 3.3 W/m$^2$, and it is 1.75 kg higher than the single slope solar still on 3-6-2020. From the comparisons of daily average EHTC and daily condensed water production, it is clear that the condensed water form on the collector surface strongly depends on both EHTC and collector surface temperature.

The relation between the temperature gradient of the basin water and the inner face of the glass and the amount of distilled water produced is a direct relationship. The higher temperature difference between basin water and the inner face of the glass has produced maximum distilled water productivity. In addition, it has been noted that the difference between Tb.w and Tc.c evident in the amount of condensed water generated from the hemispherical solar still is higher than the single slope solar still.

This is mainly due to the fact that the design of the spherical distillate shape causes an increase in the evaporation rate. In fact, the hemispherical cover causes sunlight to fall into the basin from all the directions, and then condensation rate increases and hence produces maximum condensed water as compared to the single slope solar still.

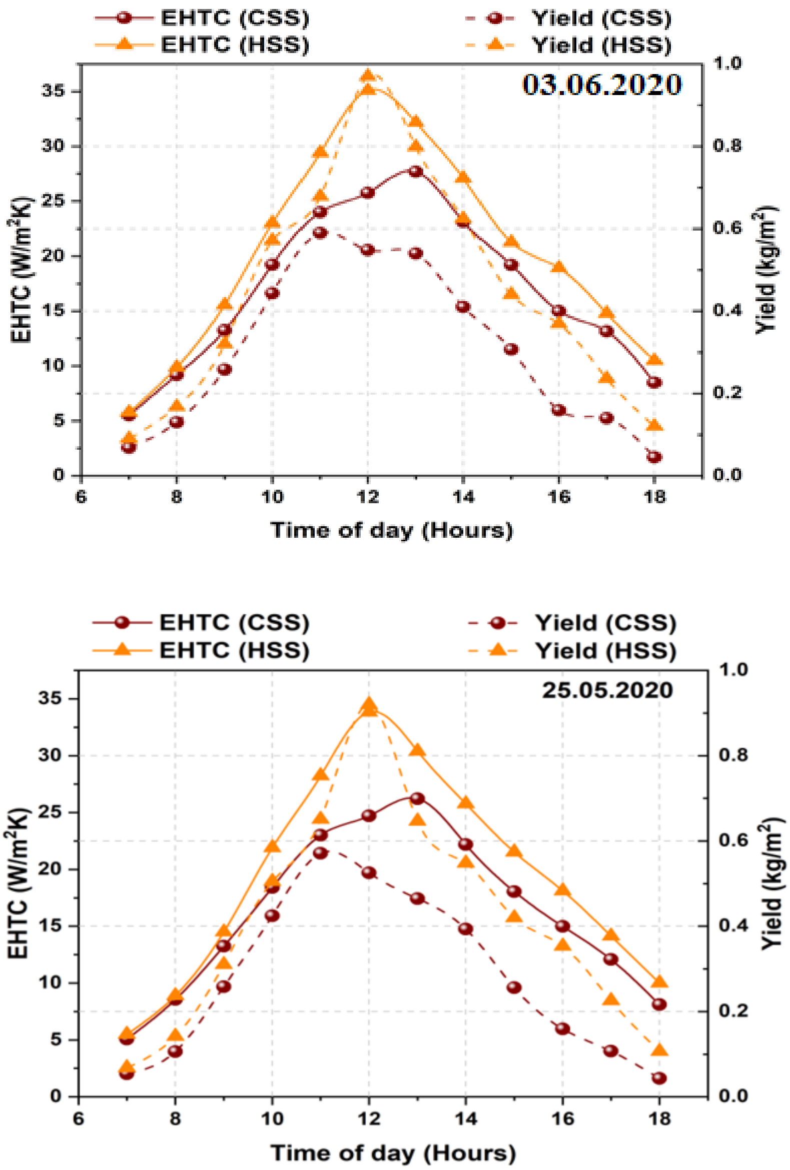


**Figure (3.5):** Time-wise changes of EHTC and condensed water production for the single slope solar still and hemispherical solar still, on 25-5-2020 and 3-6-2020

### 3.5.3. Time-wise changes of energy and exergy efficiency:

Figure (3.6) representing daily energy and exergy efficiency for the single slope solar still and hemispherical solar still. The maximum energy efficiency of the single slope solar still is 36.98% on 25-5-2020 and 38.08% on 3-6-2020. Similarly, the maximum energy efficiency of the hemispherical solar still is 56.91% on 25-5-2020 and 58.04% on 3-6-2020. The maximum energy efficiency of the hemispherical solar still is 19.94% higher than the single slope solar still on 25-5-2020 and 19.96% higher than the single slope solar still on 3-6-2020. The calculated daily average energy efficiency of the single slope solar still on 25-5-2020 is 23.74%, on 3-6-2020 is 25.81%. Likewise, the daily average energy efficiency of the HSS on 25-5-2020 is 35.96%, and on 3-6-2020 is 38.61%. The daily average energy efficiency of the hemispherical solar still is 12.2% higher than the single slope solar still on 25-5-2020 and 12.8% higher on 3-6-2020. In the hemispherical solar still, water temperature, EHTC and condensed water production are augmented and hence hemispherical solar still produced higher energy efficiency than the single slope solar still.

The maximum exergy efficiency of the single slope solar still is 2.92% on 25-5-2020 and 3.46% on 3-6-2020. Similarly, maximum exergy efficiency of the hemispherical solar still is 6.06% on 25-5-2020 and 6.5% on 3-6-2020. The maximum exergy efficiency of the hemispherical solar still is 3.14% higher than the single slope solar still on 25-5-2020 and 3.04% higher than the single slope solar still on 3-6-2020. The calculated daily average exergy efficiency of the single slope solar still on 25-5-2020 is 1.6%, and on 3-6-2020 is 1.8%. Likewise, the daily average exergy efficiency of the hemispherical solar still on 25-5-2020 is 2.7%, and on 3-6-2020 is 3.1%. The daily average exergy efficiency of the hemispherical solar still is 1.17% higher than the single slope solar still on 25-5-2020 and 1.28% higher than the single slope solar still on 3-6-2020. The exergy efficiency of the still is maximum for the hemispherical solar still because exergy efficiency directly related to condensed water production and available radiation. During the sunset time, the variation between Ts.w and Tc.c is higher so that exergy efficiency during sunset time is higher as compared to the morning. The design of the still is one of the important parameters for higher condensed water production, energy and exergy efficiency. In the hemispherical solar still, the amount of radiation falling to the basin is maximum as compared to the SSSS also condensation area for the hemispherical solar still is slightly higher as compared to the condensation area of the single slope solar still. Due to the special design (hemispherical solar still) the performance of the hemispherical solar still is superior to single slope solar still in terms of the Ts.w, condensed water production, energy and exergy efficiency.

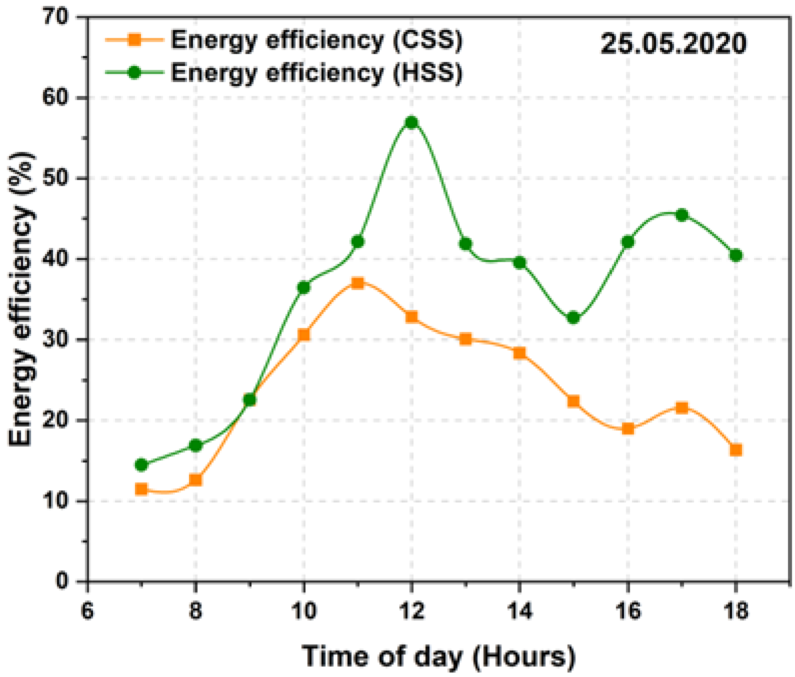


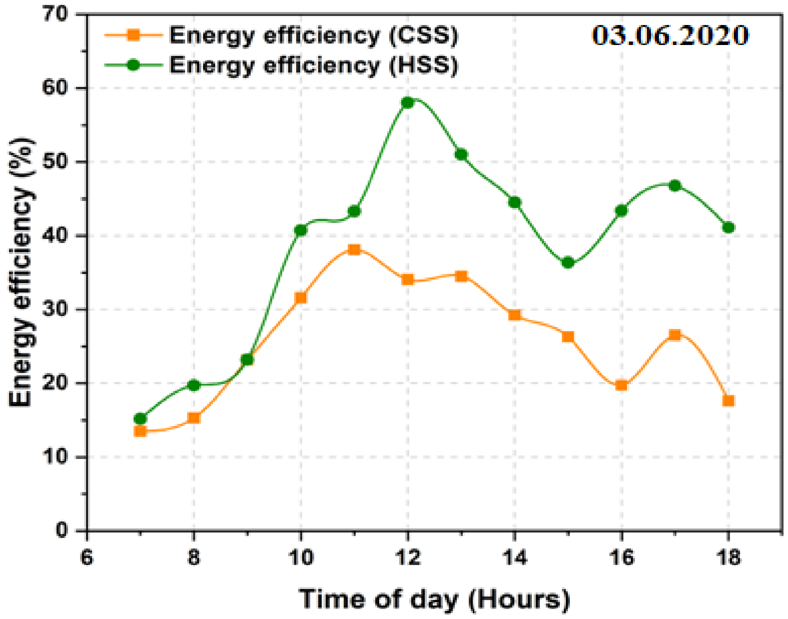

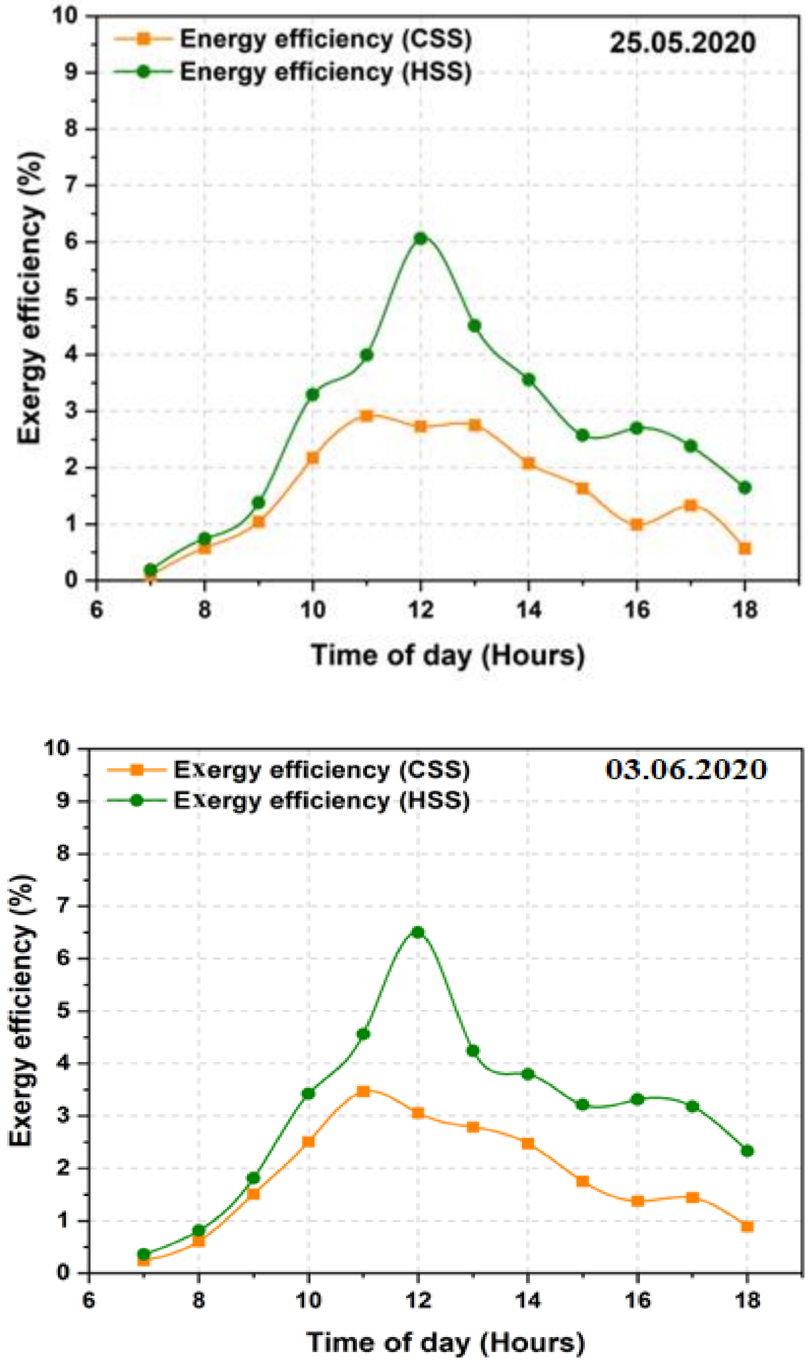


**Figure (3.6):** Time-wise changes of energy and exergy efficiency for the single slope solar still and hemispherical solar still on 25-5-2020 and 3-6-2020.

## 3.6. A rendering of daily productivity of the present study on various still designs:

A rendering of distilled water production from our study and various published solar still designs are tabulated in Table (3.3). From the table, it is pinpoint that yield produced from the single slope solar still is minimum (2.1 kg/m$^2$/day) (Phadatare and Verma, **2007**) and yield produced from the PV/T integrated solar still (5.5 kg/m$^2$/day) (Gaur and Tiwari, **2010**) and hemispherical solar still (5.71 kg/m$^2$/day) (Ismail, **2009**) is maximum. In the present investigation, distilled water production from the single slope solar still is 3.64 and from hemispherical solar still is 5.38, which is 0.3 kg less than the work carried out by (Ismail, **2009**) work.

**Table (3.3):** A rendering of the yields of various published solar still designs and present study.

| S.N° | Type of solar still | Authors name and reference | Productivity kg/m²/day | The % of the increase in productivity compared to our results |
|---|---|---|---|---|
| 1 | Single slope | Phadatare and Verma, (**2007**) | 2.10 | 156.20 |
| | | Samee et al., (**2007**) | 3.42 | 57.30 |
| 2 | Double slope | Rajamanickam and Ragupathy, (**2012**) | 3.07 | 75.24 |
| | | Aburideh et al., (**2012**) | 4.00 | 34.50 |
| 3 | Pyramid | Taamneh and Taamneh, (**2012**) | 2.83 | 90.10 |
| | | Manokar et al., (**2019**) | 3.70 | 45.40 |
| 4 | Inclined | Hansen et al., (**2015**) | 4.18 | 28.70 |
| | | El-Agouz et al., (**2015**) | 4.54 | 18.50 |
| 5 | Tubular | Ahsan et al., (**2012**) | 4.60 | 16.95 |
| | | Tiwari and Kumar, (**1988**) | 5.00 | 07.60 |
| 6 | PV/T integrated | Kumar and Tiwari, (**2010**) | 5.24 | 03.30 |
| | | Gaur and Tiwari, (**2010**) | 05.5 | -02.18 |
| 7 | "V" type | Suneesh et al., (**2014**) | 4.60 | 16.95 |
| | | Kumar et al.,(**2008**) | 4.33 | 24.25 |
| 8 | Hemispherical | Arunkumar et al., (**2012**) | 4.20 | 28.10 |
| | | Ismail, (**2009**) | 5.71 | -05.78 |
| 9 | Single slope | Present study | 3.64 | 47.80 |
| | Hemispherical | Present study | 5.38 | - |

## 3.7. A rendering energy and exergy efficiency of our study with previous research works:

Table (3.4) summarizes the rendering of energy and exergy efficiency of the hemispherical solar still of our study with previous research works. According to our experimental study, the maximum daily average exergy efficiency of the single slope solar still is equal to 25.81% and 38.61% for the hemispherical solar still. The daily average exergy efficiency of the single slope solar still is 1.28% lesser than the hemispherical solar still.

**Table (3.4):** A rendering of energy and exergy efficiency of the single slope solar still and hemispherical solar still with previous research works.

| S.N° | Type of solar still | Authors name and reference | Energy efficiency (%) | Exergy efficiency (%) |
|---|---|---|---|---|
| 1 | Single slope | Attia et al., (**2020b**) | 52.50 | 1.20 |
| 2 | Inclined | Monakar et al., (**2018**) | 39.82 | 2.90 |
| 3 | Single slope | Sakthivel and Arjunan, (**2019**) | 23.80 | 2.60 |
| 4 | Single slope | Attia et al., (**2020c**) | 33.40 | 1.80 |
| 5 | Single slope | Vaithilingam and Esakkimuthu, (**2015**) | 30.97 | 3.48 |
| 6 | Single slope | Attia et al., (**2021a**) | 33.10 | - |
| 7 | Single slope | Present study | 25.81 | 1.84 |
| | Hemispherical | Present study | 38.61 | 3.13 |

## 3.8. Economic evaluation:

An economic study is necessary to know the profitability of the project and know the number of days to recover the money invested in the project. For this, the costs of the hemispherical solar still and the single slope distillate were compared. In these conditions, we have taken into account our economic calculations of several parameters, such as manufacturing cost, maintenance cost, daily productivity of distilled water, and the selling price of one liter of distilled water. Table (3.5) compares the cost of manufacturing of the single slope solar still and the hemispherical solar still, knowing that the cost per liter of the distilled water on the market is equal to 0.45 $. So, the calculation of the number of days to recover the funds invested in the project for both single slope solar still and hemispherical solar still distilleries, after subtracting maintenance cost is presented. From these results, it has been concluded that the hemispherical solar still is profitable compared to the single-slope distillation machine even economically.

**Table (3.5):** Fabrication cost of the single slope and hemispherical solar still.

| Type of solar still | Single slope | Hemispherical |
|---|---|---|
| Total cost of manufacture ($) | 60.57 | 68.14 |
| Maintenance cost ($) | 0.38 | 0.38 |
| Total cost ($) | 60.95 | 68.52 |
| The amount of water produced during the day (kg/m$^2$/d) | 3.64 | 5.38 |
| The cost per liter of distilled water on the market ($) | 0.45 | 0.45 |
| The price of daily water production ($) | 1.64 | 2.43 |
| Recovery period (Days) | 37 Days | 28 Days |

## 3.9. A comparative of the conventional distiller (hemispherical and single slope):

According to our experimental study, the maximum productivity is equal to 3.64 kg/m$^2$/day for the single slope solar still and 5.38 kg/m$^2$/day for the hemispherical solar still. The maximum daily energy efficiency of the single-slope design is 25.81%, and hemispherical design is 38.61%. Similarly, the maximum daily exergy efficiency of single-slope design still is 1.8%, and hemispherical designed solar still is 3.1%. When comparing the characteristics of the hemispherical distillation apparatus with the conventional single-slope distillation machine, we note that hemispherical solar still is characterized by a large area of reception and condensation compared to single slope solar still. It is for this feature and for the benefit of it we compare each: productivity, the number of days to recover, energy and exergy efficiency. Table (3.6) summarizes the major outcomes of the present comparative study. The main conclusion from our experimental study is the hemispherical distillery greatly enhances the productivity as compared to the single slope distillate and gives more energy and exergy efficiency.

**Table (3.6):** Productivity, the number of days to recover, energy and exergy efficiency of the single slope solar still and hemispherical solar still.

| Date | Productivity (kg/m²/day) | | The % of the increase in productivity compared to HSS and SSSS. | Energy efficiency (%) | | Exergy efficiency (%) | | Recovery period (Days) |
|---|---|---|---|---|---|---|---|---|
| | SSSS | HSS | | SSSS | HSS | SSSS | HSS | SSSS |
| 25-5-2020 | 3.36 | 4.9 | 45.83 | 23.74 | 35.96 | 1.57 | 2.75 | 40 |
| 3-6-2020 | 3.64 | 5.38 | 47.80 | 25.81 | 38.61 | 1.84 | 3.13 | 37 |

## 3.10. Conclusion:

In this chapter, the performance of the single slope solar still and hemispherical solar still was evaluated experimentally. The experiments were conducted on 25-5-2020 and 3-6-2020 continuously for 11 hours from 7 AM to 6 PM. Based on the obtained results, the following outcomes are achieved:

- The results show that the hemispherical solar still gave 5.38 kg/m$^2$/day of yield for the duration of the experiment, whereas the single-slope solar distillery was given 3.64 kg/m$^2$/day.
- There is an improvement in the daily yield from the hemispherical solar still by 48% compared to the daily productivity of the single slope solar still.
- The daily accumulation of the hemispherical solar still has increased by 1.48 times, compared to the daily accumulation of the single-slope distillate.
- The maximum overall energy and exergy efficiencies were 38.6% and 3.1% for hemispherical solar still and 25.8% and 1.8% for the single slope solar still.
- We can recover the total cost of single slope solar still in 37 days, while of hemispherical solar still in 28 days, although total cost of hemispherical solar still is more expensive than single slope solar still.

# Chaptre 04 :

# Productivity enhancement of hemispherical solar still using $Al_2O_3$-water-based nanofluid and cooling the glass cover

## 4.1. introduction:

The hemispherical solar distillers are characterized by having large receiving/condensing surface area as compared to conventional single-slope distillers. Previous studies showed that the effect of nanoparticles raise the temperature at midday. The present experimental study aims to enhance the hemispherical solar distiller performance. To achieve this idea, two modifications was done on the hemispherical distiller, namely (i) use $Al_2O_3$ nanoparticles with different concentrations (0.1, 0.2, and 0.3%) to increase the evaporation rate, (ii) use of glass cover cooling technology by the water sprinkler to increase the condensation rate. To investigated the influences of $Al_2O_3$-water nanofluid and the glass cover cooling technology by water sprinkler on hemispherical solar distiller performance. three hemispherical solar distillers were designed, constructed, and tested at the same climate conditions. The first is the conventional hemispherical distiller which represents the reference case, the second is the modified hemispherical distiller with $Al_2O_3$- water nanofluid, and the third is the modified hemispherical solar distiller with $Al_2O_3$- water nanofluid and the water sprinkler.

## 4.2. Aluminum oxide nano-particles preparation method:

In general, the Sol–Gel (Elaloui and Pajonk, **2000**) process is a simple method for collecting nano materials, in the recent period many metal oxides have been synthesized such as $SiO_2$ (Pajonk et al., **1996**), $Al_2O_3$ (Ponthieu et al., **1993**; Elaloui et al., **1997**), ZnO (Elaloui et al., **2002**), $TiO_2$ (El-Mir et al., **2008**; Elghniji et al., **2012**), $Co/SiO_2$ nano composites (Fouad et al; 2011), $Co_3O_4$/ $SiO_2$ nano composites (Ali et al., **2013**), $Al_2O_3$ thin films (Hu et al., **2016**). etc. The sol-gel method is used for the synthesis of alumina in which an inorganic material is polymerized around the micelle of the surfactant (Kachbouri et al., **2019**). And to follow this method see Figure (4.1).

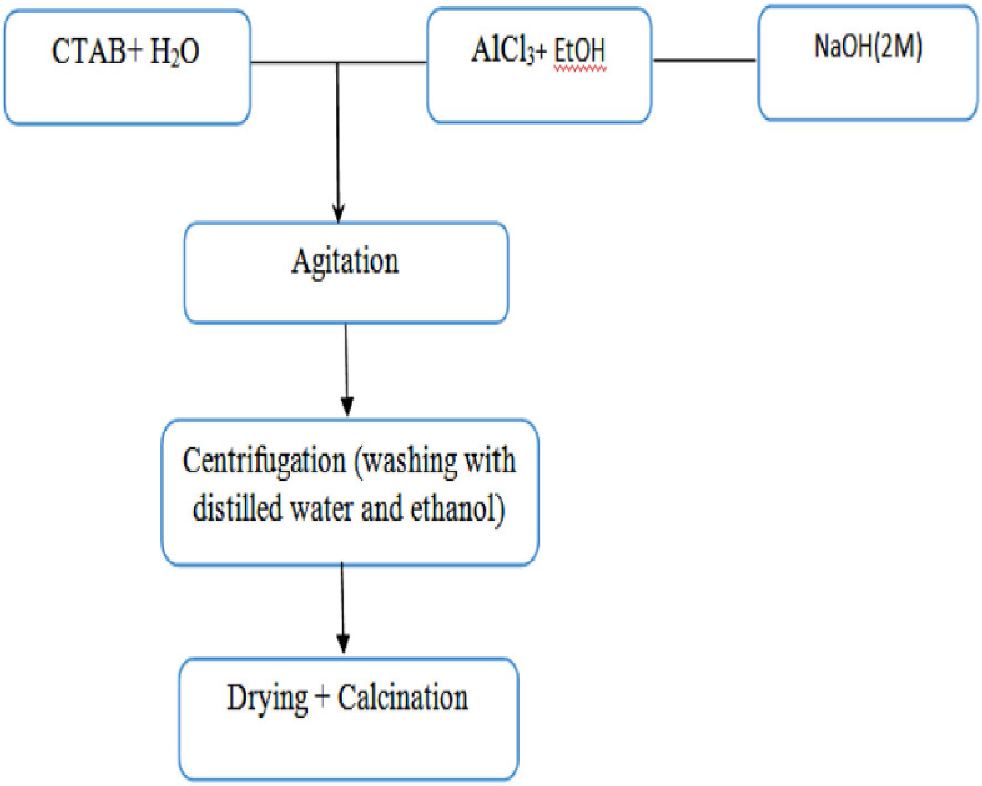


**Figure (4.1):** Flowchart of the modified sol–gel

### 4.2.1. Infrared characterizations:

Alumina was characterized by infrared radiation in Figure (4.2) and the characteristic peak was observed in 635, 739, and 1450 cm$^{-1}$ corresponding to Al-O, Al-O-Al, and Al-Al (Tabesh et al., **2018**; Zhang et al., **2016**). Also, the peak is at 1630 cm$^{-1}$ for the HOH (Peng et al., **2016**) The peak is at 2500 cm$^{-1}$ (2490 cm$^{-1}$) due to the absorption of carbon dioxide into the atmosphere (Farahmandjou and Motaghi, **2019**) Also, there is a wide band at 3500 cm$^{-1}$ in the group O-H (Tangsir et al., **2015**).

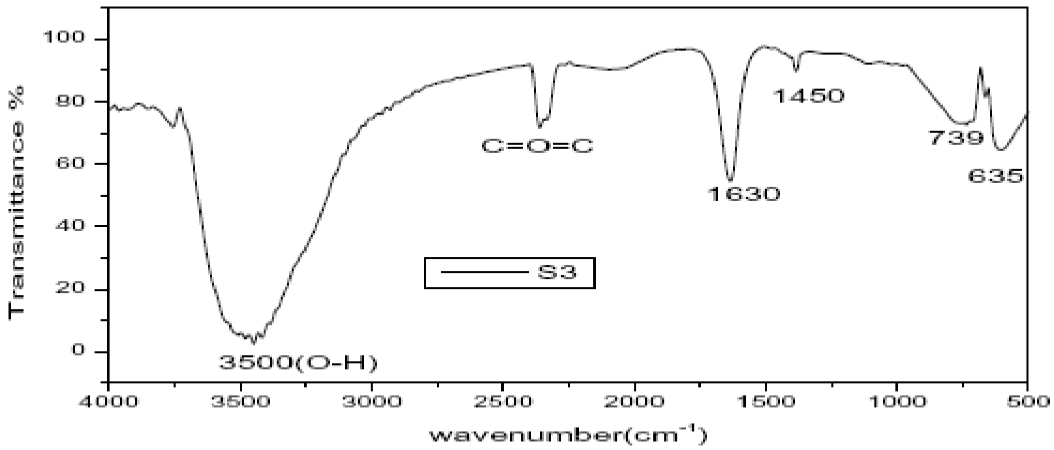


**Figure (4.2):** The infrared spectrum of aluminum

## 4.2.2. Scanning electron microscopy (SEM):

The SEM image of $Al_2O_3$ sample is illustrated in Figure (4.3) EDX analyses were performed on this (S3) sample to demonstrate the chemical composition of $Al_2O_3$ shown in Figure (4.3) and Table (4.1).

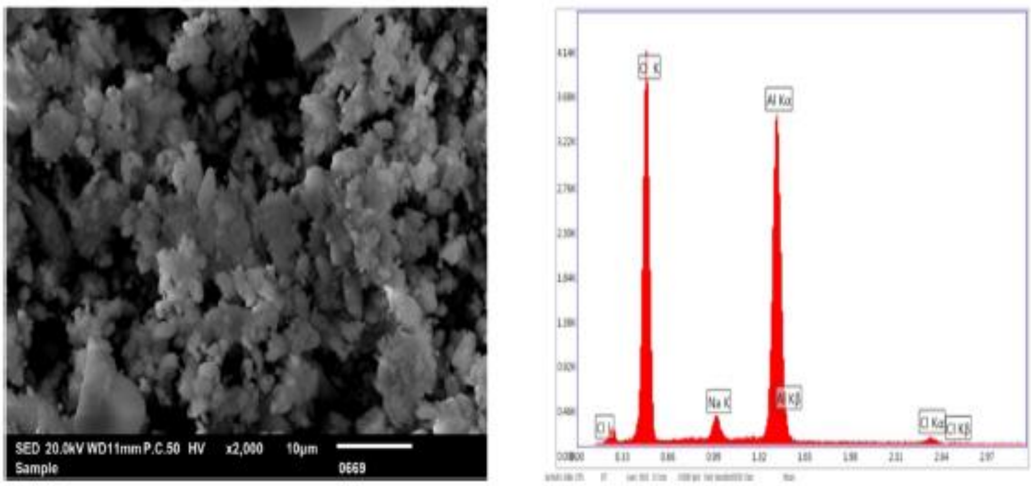


**Figure (4.3):** SEM image of the sample.

**Table (4.1):** Alumina chemical composition.

| Elements | (%) |
|---|---|
| Al | 55.02 |
| O | 37.96 |
| Cl | 3.75 |
| Na | 3.27 |

## 4.3. Experimental setup:

In present experimental setup, three fixed hemispherical distillers were designed and constructed to obtain the influences of $Al_2O_3$- water nanofluid and cooling technology of glass cover by water sprinkler on the accumulative yield of hemispherical distillers. The three distillers were classified as followed; the first is the conventional hemispherical solar distiller (CHSS) which represents the reference case, the second is the modified hemispherical solar distiller with $Al_2O_3$-water based nanofluids (MHSSN), and the third is the modified hemispherical solar distiller with $Al_2O_3$- water based nanofluid and the water sprinkler (MHSSNS). Figure (4.4), Figure (4.5) shows the schematic diagram and photographic view of experimental test-rig. As shown in Figure (4.4) each hemispherical solar basin of 0.1 $m^2$ basin area. The basin of the hemispherical distiller was formed with a 38 cm diameter and 25 mm depth within a wooden board. The inner walls of the basin are coated with black silicon to increase absorption capacity. The basin is covered with a 3 mm thick transparent plastic cover. Table (4.2) shows the specifications of the $Al_2O_3$ nanoparticles.

The experimental test rig consists from a three hemispherical distillers; the first is the conventional hemispherical solar distiller (CHSS) which represents the reference case, the second is the modified hemispherical solar distiller with $Al_2O_3$-water based nanofluid (MHSSN), and the third is the modified hemispherical solar distiller with $Al_2O_3$- water-based nanofluid and the water sprinkler (MHSSNS). The basin working fluid utilized in the conventional hemispherical distiller is a pure water, but in a modified hemispherical distiller, the basin working fluid is $Al_2O_3$-water nanofluid with volume fraction 0.1, 0.2, and 0.3%. The $Al_2O_3$- water nanofluid was prepared, using 500 W Probe sonicator and 1% Ascorbic acid ($C_6H_8O_6$) as the surfactant. A2-week sedimentation test was used to check the stability and it was observed that the nanoparticles are well dispersed as even after 2 weeks.

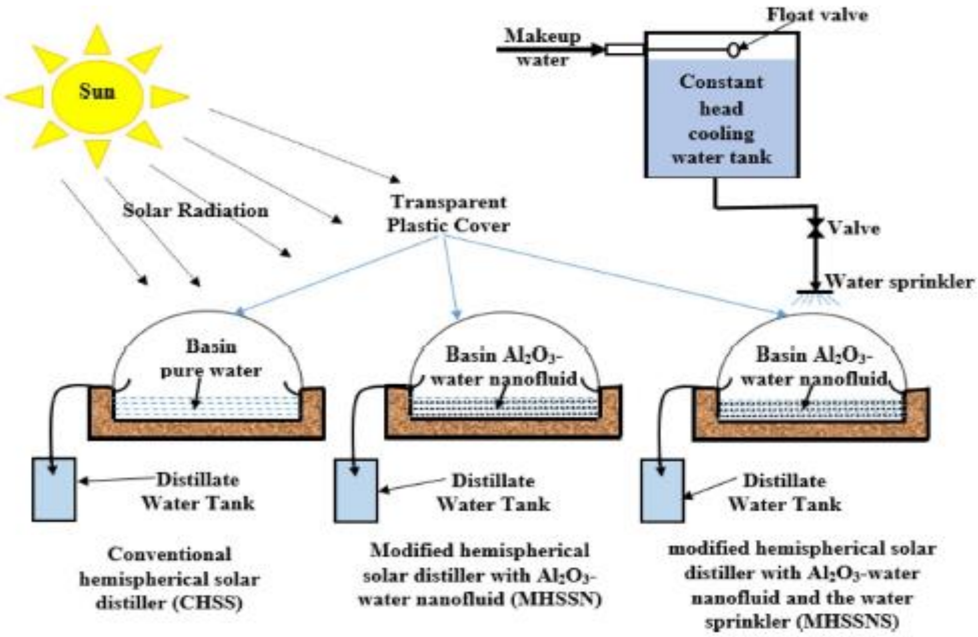


**Figure (4.4):** Schematic diagram of experimental test rig.

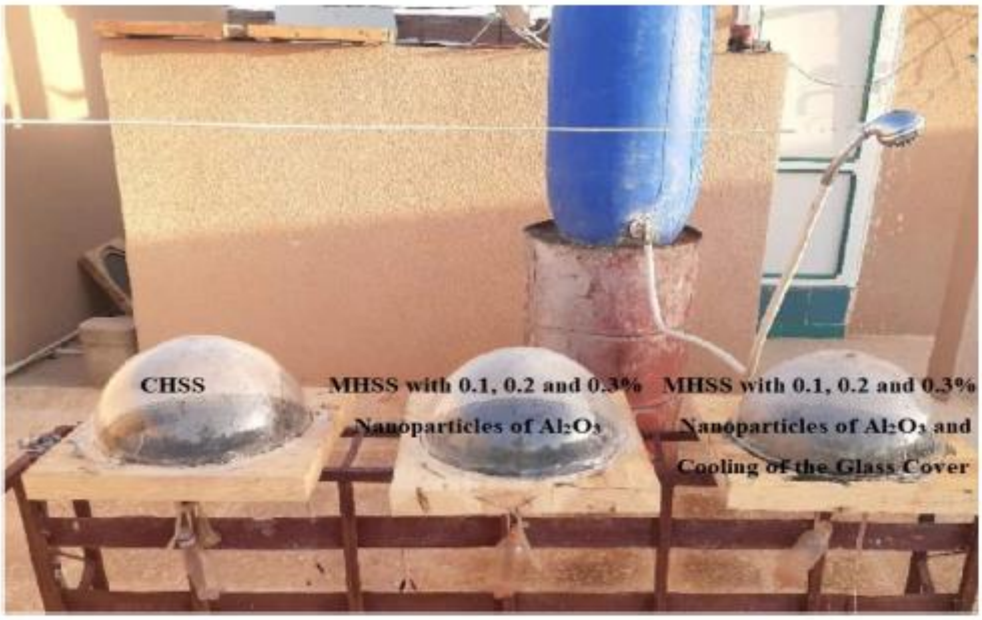


**Figure (4.5):** A photographic view of experimental test rig.

**Table (4.2):** Specifications of $Al_2O_3$ nanoparticles.

| Specifications | Nanoparticles of $Al_2O_3$ |
|---|---|
| Thermal conductivity, W/(mK) | 38.5 |
| Density, g/cm$^3$ | 3.89 |
| Specific heat, Cp, J/kgK | 880 |
| Average particles size, nm | 3–5 |

## 4.4. Experimental procedure:

The experiments were conducted for a period of three days in a row: 25, 26 and 27 September 2020 for 10 hours in the city of El Oued Algeria located at 06° 47′ E and 33° 30′ N. In the experiments, the experimental data recorded for the three hemispherical distillers [(i) conventional hemispherical distiller (CHSS), (ii) modified hemispherical distiller with $Al_2O_3$- water nanofluid (MHSSN), and (iii) modified hemispherical distiller with $Al_2O_3$- water nanofluid and the water sprinkler (MHSSNS)] at the same weather conditions. In our tests, three concentrations of aluminum oxide nanoparticles equal to 0.1, 0.2, and 0.3% were considered for three consecutive days as shown in Table (4.3) .The cover glass is cooled by water sprinkler a constant rate of 0.008 kg/s (MHSSNS).

**Table (4.3):** The different used test configuration.

| Case | | Method |
|---|---|---|
| Conventional | CHSS | Conventional Hemispherical Solar Still |
| Case (A) | MHSSN | Modified Hemispherical Solar Still $Al_2O_3$- water nanofluid (0.1%). |
| Case (B) | | Modified Hemispherical Solar Still $Al_2O_3$- water nanofluid (0.2%). |
| Case (C) | | Modified Hemispherical Solar Still $Al_2O_3$- - water nanofluid (0.3%). |
| Case (A2) | MHSSNS | Modified Hemispherical Solar Still $Al_2O_3$- water nanofluid (0.1%) and water sprinkler (0.008 kg/s). |
| Case (B2) | | Modified Hemispherical Solar Still $Al_2O_3$- water nanofluid (0.2%) and water sprinkler (0.008 kg/s). |
| Case (C2) | | Modified Hemispherical Solar Still $Al_2O_3$- water nanofluid (0.3%) and water sprinkler (0.008 kg/s). |

The empirically test-rig is suitably equipped to measure brine and absorbent temperatures and cover glass temperatures at different points of distillation. The total solar irradiance and the amount of distilled water are also taken into consideration.

Temperatures are measured in thermocouples and the solar intensity is measured instantly with a solarimeter. Table (4.4) shows error values committed in measuring devices.

**Table (4.4):** Accuracy and standard uncertainties.

| Device | Range | Accuracy | Standard uncertainty |
|---|---|---|---|
| Solar power meter | 0–1999 W/m$^2$ | ±10 W/m$^2$ | 5.72 W/m$^2$ |
| Thermocouple | −100 – 500°C | ± 0.1°C | 0.07°C |
| Graduated cylinder | 0 – 250 ml | ± 1 ml | 0.6 ml |

## 4.5. Result and discussion:

Solar radiation is the most important environmental factor in distillate process. Figure (4.6) shows the variations of both recorded weather temperature and solar intensity with time on the three selected working days starting 8:00 am–6:00 pm. It should be noted that both air temperature and solar intensity trends are oneself for the three working days during the period from 8:00 am to 6:00 pm. Ambient air temperatures varying between 30 and 38°C, 30–42°C, and 30–41°C for the test days from 15 to 17 Sep 2020, respectively. The maximum values of solar intensity at 12:00 am were recorded 1006 W/m$^2$ for the 3 tested days.

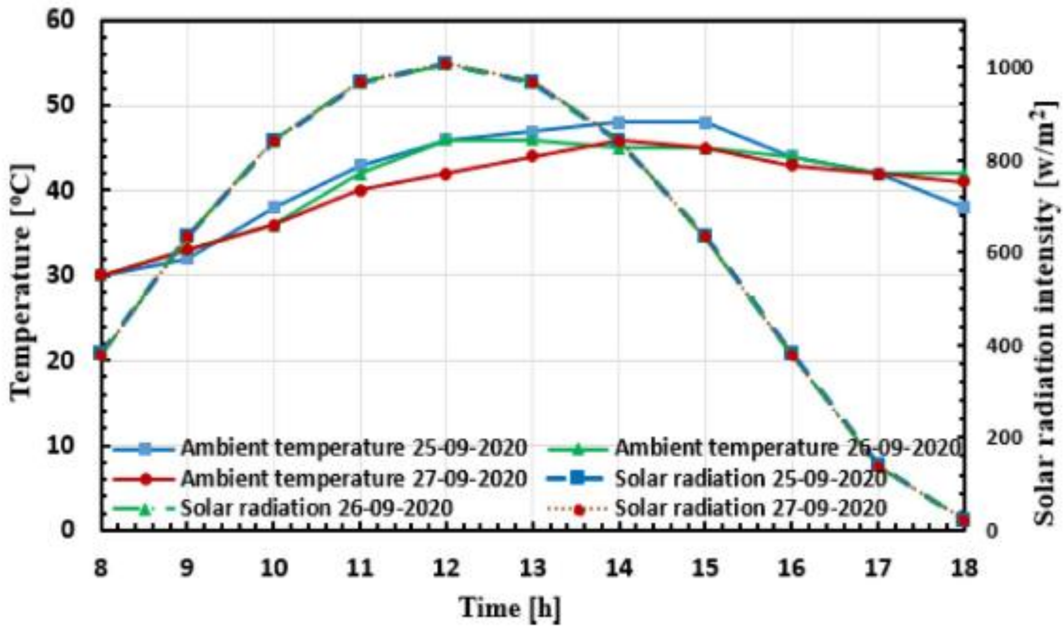


**Figure (4.6):** Weather temperature and solar energy variations through three test days.

The effect of utilization $Al_2O_3$- water nanofluid and water sprinkler on the basin water (or nanofluid) temperature are shown in Figure (4.7). As shown, the basin temperatures for the modified hemispherical solar stills with $Al_2O_3$- water nanofluid and water sprinkler are higher than that of traditional hemispherical solar distiller. The water basin temperature for traditional hemispherical distiller varies between 30 and 60°C along the day. The basin nanofluid temperature of modified hemispherical solar distillers $Al_2O_3$- water nanofluid varies between 31 and 63°C, 30–64°C, and 30–66°C for cases (A), (B), and (C), respectively. On the other hand, the basin nanofluid temperature for modified hemispherical solar distillers utilizing the $Al_2O_3$- water nanofluid and water sprinkler varies between 31 and 62°C, 30–63°C, and30–66°C for cases (A2), (B2), and (C2), respectively.

The higher temperatures of the basin nanofluid for the modified hemispherical solar distillers is because the higher in the intensity of absorbed solar radiation, as well as the improvement in the thermal properties due to adding the $Al_2O_3$ nanoparticles to the basin water as compared to CHSS.

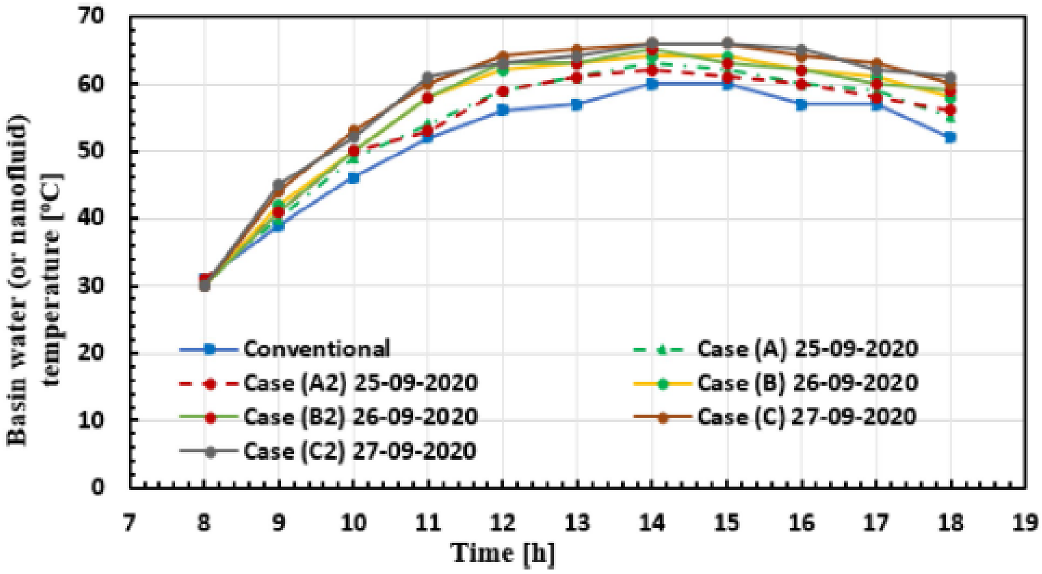


**Figure (4.7):** Variation of water (or nanofluid) basin temperature along daytime of the CHSS, MHSSN, and MHSSNS through the three tested days.

Figure (4.8), Figure (4.9) present the variations of internal/external glass side temperatures along daytime of conventional and modified hemispherical solar still with $Al_2O_3$-water nanofluid and water sprinkler through the 3 tested days starting8:00 am–6:00 pm. As shown, the internal glass side temperature for conventional hemispherical solar still varies between 30 and 53°C and external glass side temperature varies between 30 and 50°C. The internal glass side temperatures of the modified hemispherical solar still for cases (A), (B), and (C) varies between 30 and 53, 29–54, and29–55°C with $Al_2O_3$- water nanofluid and between 27 and48, 29–50, and 28–51°C for cases (A2), (B2), and (C2) with $Al_2O_3$-water nanofluid and water sprinkler, respectively. On the other hand, the external glass side temperatures of the modified hemispherical solar distiller for cases (A), (B), and (C) varies between 30 and 50, 29–50, and 29–50°C and for cases (A2), (B2), and (C2) varies between 28 and 48, 27–46, and 27–46°C, respectively. The amount of decreases in the internal and external glass side temperature of glass cover varying between 2 and 7°C in the case of utilizing the glass cover cooling technology in a modified hemispherical distiller with $Al_2O_3$- water nanofluid and water sprinkler, and this is a good indication of an increase in the condensation rate and consequently an improvement in distillate water productivity.

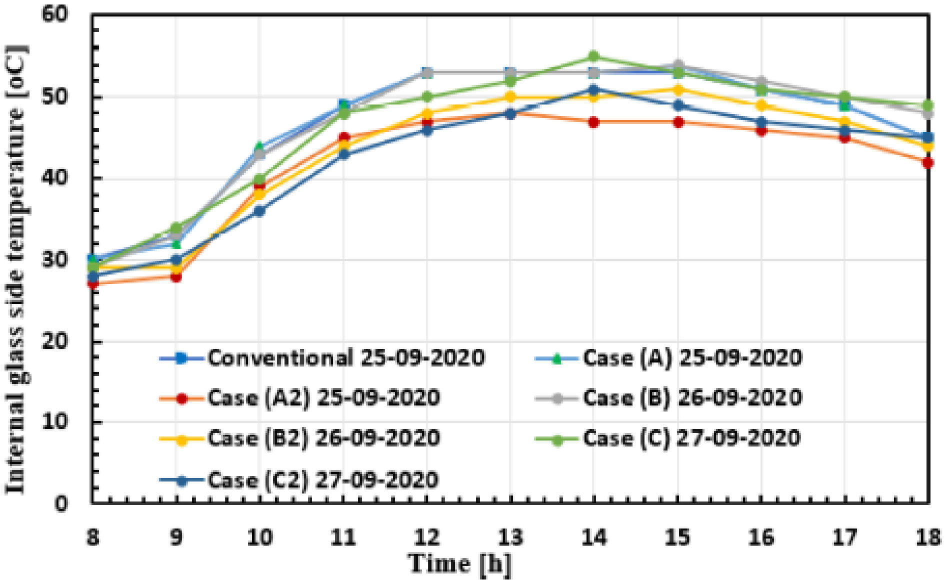


**Figure (4.8):** Variation of internal glass side temperature along daytime of the CHSS, MHSSN, and MHSSNS through the three test days.

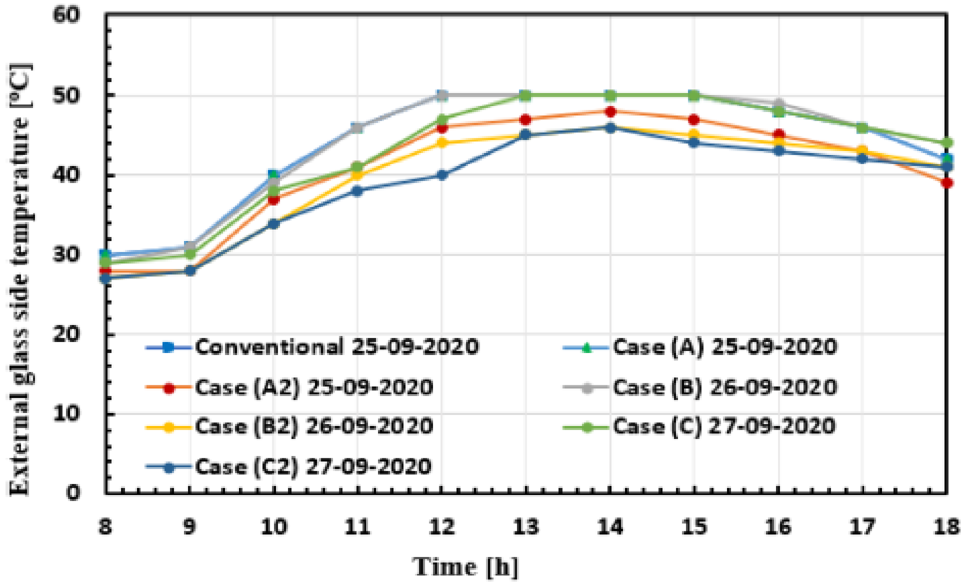


**Figure (4.9):** Variations of external glass side temperature along daytime of the CHSS, MHSSN, and MHSSNS through the three test days.

The variation of hourly distillated water for traditional and modified hemispherical solar distiller with $Al_2O_3$- water nanofluid and water sprinkler along the day is presented in Figure (4.10). The hourly distillated water for the conventional hemispherical solar still varies between 0 and 450 ml/m$^2$h along the day (8:00 am–6:00 pm). Hourly distillated water of modified hemispherical solar still for cases (A), (B), and (C) is varies between 0 and 650, 0–700, and 0–750 ml/m$^2$h along the day (8:00 am–6:00 pm) and for cases (A2), (B2), and (C2) varies between 0 and 900, 0–920, and 0–950 ml/m$^2$h, respectively.

The maximum yield for conventional hemispherical solar still up to 450 ml/m$^2$h, for modified hemispherical distiller cases (A), (B), and (C) is 650, 700, 750 ml/m$^2$h, respectively and for cases (A2), (B2), and (C2) is 900, 920, 950 ml/m$^2$h, respectively, are obtained at 14:00 pm for all cases. As presented in this figure, the yield of the modified hemispherical solar still with $Al_2O_3$- water nanofluid and water sprinkler [cases (A2), (B2), and (C2)] are higher compared the conventional and modified hemispherical solar still with $Al_2O_3$- water nanofluid [cases (A), (B), and (C)].

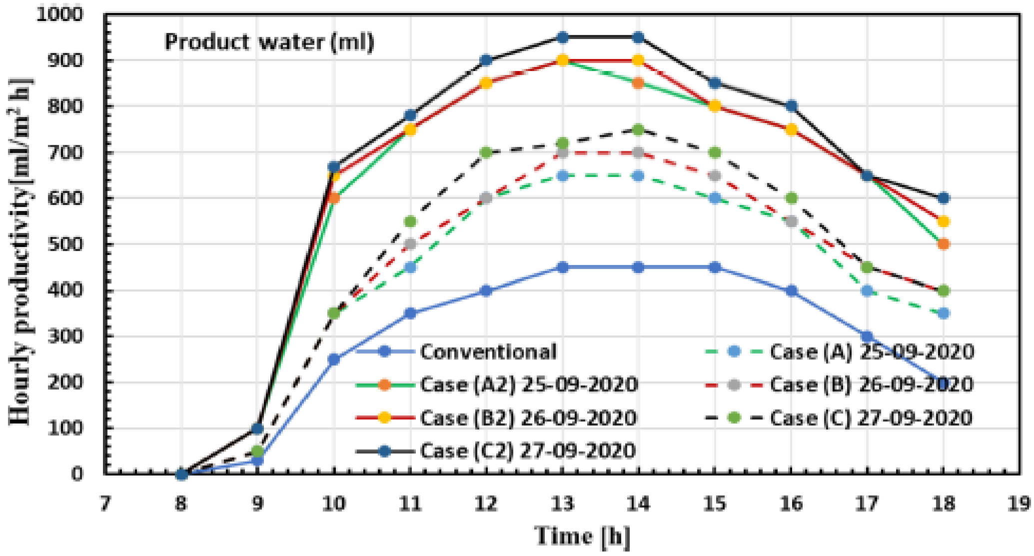


**Figure (4.10):** Variation of productivity per-hourly for the CHSS, MHSSN, and MHSSNS through the three test days.

Figure (4.11) shows the accumulative yield of traditional hemispherical distiller, modified hemispherical distiller with $Al_2O_3$- water nanofluid [cases (A), (B), and (C)], and modified hemispherical distiller with $Al_2O_3$- water nanofluid and water sprinkler [cases (A2), (B2), and (C2)]. The accumulative yield of conventional hemispherical solar still reached 3280 ml/m$^2$, will utilizing the $Al_2O_3$-water nanofluid improve the accumulative yield to 4650, 4950, and 5270 ml/m$^2$ with improvement 41.8, 50.9, and 61.3% for cases (A), (B), and (C), respectively, as compared to CHSS. In addition, the utilization of the water sprinkler in cooling a cover of the modified hemispherical distiller with $Al_2O_3$-water nanofluid will be improve the accumulative yield to 6750, 6900, and 7250 ml/m$^2$ with improvement 105.8, 110.4, and 121% for cases (A2), (B2), and (C2), respectively, as compared to CHSS.

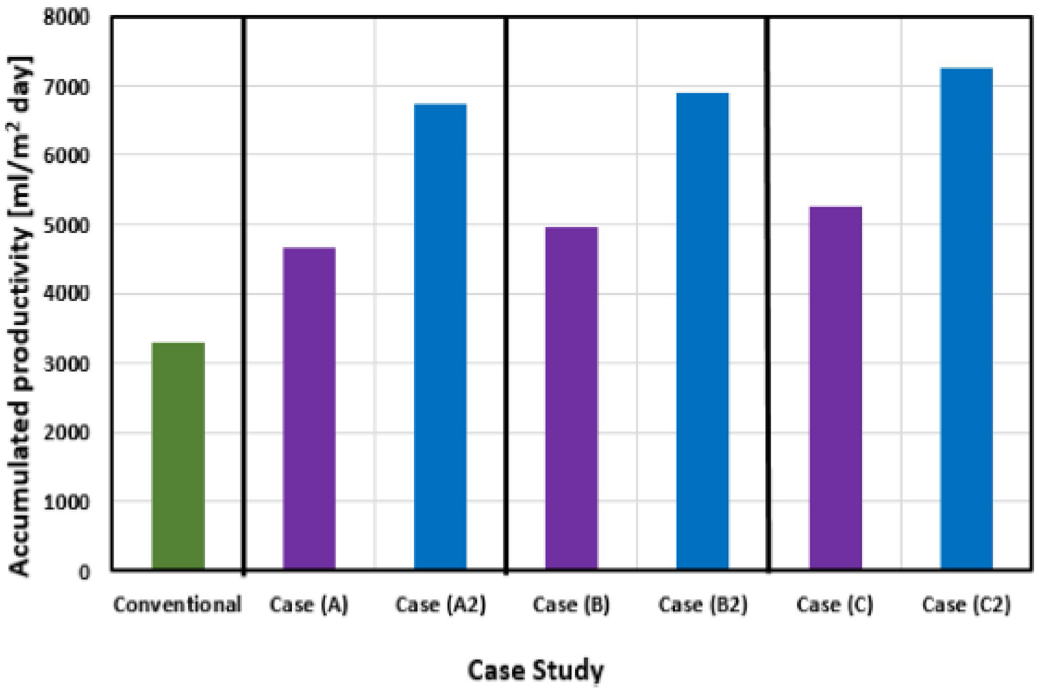


**Figure (4.11):** Accumulated daily productivity for CHSS, MHSSN, and MHSSNS.

The daily efficiency $\eta_{daily}$ of hemispherical distillers depends on accumulative yiel ($\Sigma\dot{m}_d$ ), latent heat ( $h_{fg}$ ), sum of solar radiation along a test day ( $\Sigma I(t)$ ), absorber area ( $A_s$ ) as follows:

$$\eta_{daily} = \frac{\sum \dot{m}_d \times h_{fg}}{\sum I(t) \times A_s} \quad (4.1)$$

Figure (4.12) shows the daily efficiency of traditional hemispherical distiller, modified hemispherical distiller with $Al_2O_3$- water nanofluid [cases (A), (B), and (C)), and modified hemispherical distiller with $Al_2O_3$- water nanofluid and water sprinkler (cases (A2), (B2), and (C2)]. The daily efficiency of conventional hemispherical solar still reached31.8%, will utilizing the $Al_2O_3$-water nanofluid improve the daily efficiency to 45, 47.9, and 50.9% with improvement 41.5, 50.6, and 60% for cases (A), (B), and (C), respectively, as compared to CHSS. In addition, the utilization of the water sprinkler in cooling the cover of modified hemispherical distiller with $Al_2O_3$- water nanofluid will be improve the daily efficiency to 65.4, 66.7, and 70% with improvement 105.7, 109.7, and 120.1% for cases (A2), (B2), and (C2), respectively, as compared to CHSS.

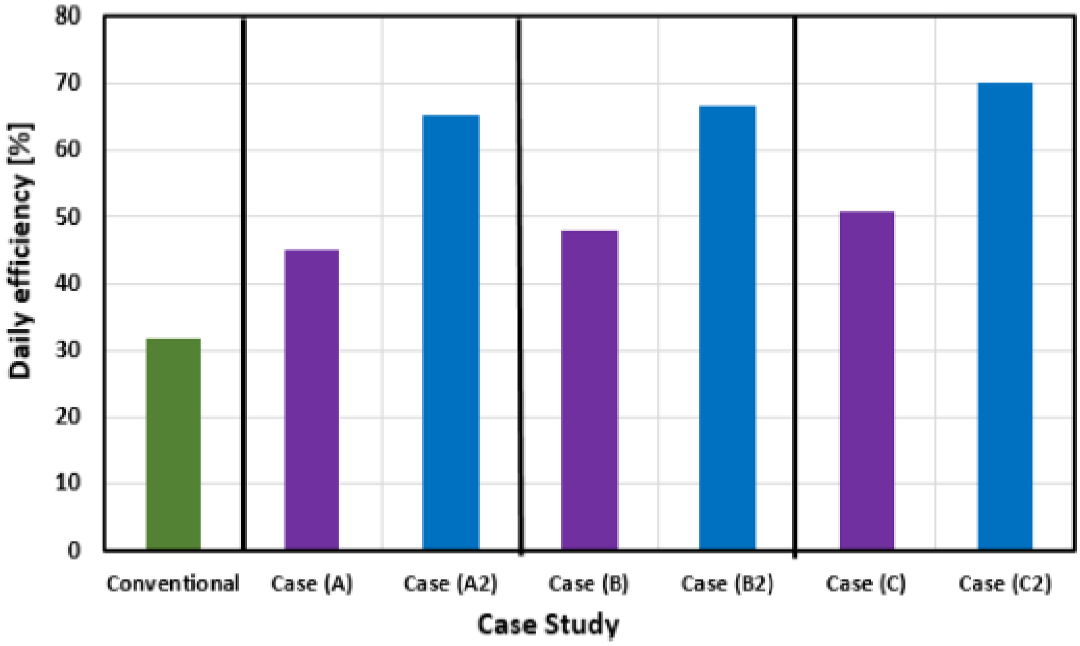


**Figure (4.12):** Daily efficiency for CHSS, MHSSN, and MHSSNS.

## 4.6. Comparison of similar studies:

Table (4.5) shows a comparison between the improvement in cumulative yield of our results with the results of another previous studies. Through the results, it is noted that the accumulative yield of a hemispherical distiller for utilizing the $Al_2O_3$- water nanofluid (0.3% concentration) improved by 61.35% compared to CHSS. Moreover, the cumulative yield improved by 121% when using $Al_2O_3$-water nanofluid (0.3% concentration) and water sprinkler compared to CHSS. Thus, $Al_2O_3$- water nanofluid and glass cover cooling greatly enhance the productivity of solar distillation.

**Table (4.5):** Compared our results with results of another previous studies.

| Authors | Solar still design | Nanoparticle | Yield improvement (%) |
|---|---|---|---|
| Kabeel et al.,(2014a) | Single slope | $Al_2O_3$ | 11.6 |
| Nijmeh et al., (2005) | Single slope | $K_2Cr_2O_7$<br>$KMnO_4$ | 17<br>26 |
| Elango et al., (2015) | Single slope | ZnO<br>$Fe_2O_3$<br>$Al_2O_3$ | 12.67<br>18.83<br>29.95 |
| Sahota and Tiwari, (2016) | Double slope | $Al_2O_3$ | 12.2 |
| Chaichan and Kazem, (2015) | Conical type | Parabolic dish with sun tracker and PCM | 307.54 |
| Chaichan and Kazem, (2018) | Single slope | Combination of paraffin wax with a nano-$Al_2O_3$ | 60.53 |
| Our study | Hemispherical | $Al_2O_3$ (0.1, 0.2and 0.3%).<br>$Al_2O_3$ (0.1, 0.2and 0.3%)and cooling of the glass cover | 41.8, 50.9, and 61.3%<br>105.8, 110.4, and 121% |

## 4.7. Economic analysis:

Based on the economic analysis in Table (4.6), it can be concluded that we can recover the cost with respect to conventional HSS after 45 days, Case (C) after 28 days, and Case (C2) after 20 days.

**Table (4.6):** Fabrication cost of the distillers CHSS, MHSSN and MHSSNS**.**

| | CHSS | Case (C) | Case (C2) |
|---|---|---|---|
| Total cost of manufacture ($) | 73.3 | 73.3 | 73.3 |
| The price of nanoparticle of $Al_2O_3$ ($) | - | 0.41 | 0.41 |
| The price of spray water ($) | - | - | 0.25 |
| Maintenance cost ($) | 0.41 | 0.41 | 0.41 |
| Total cost ($) | 73.71 | 74.12 | 74.37 |
| Accumulative yield during the day ($kg/m^2/day$) | 3.28 | 5.27 | 7.25 |
| The price of one liter on market ($) | 0.5 | 0.5 | 0.5 |
| The price of accumulative yield ($) | 1.64 | 2.635 | 3.625 |
| Recovery period (Day) | 45 Day | 28 Day | 20 Day |

## 4.8. Conclusion:

In a current study, we are interested in using $Al_2O_3$- water nanofluid with three concentrations (0.1, 0.2 and 0.3%) and cooling of the glass cover with a constant water flow rate 0.008 kg/s to achieve the highest hemispherical distiller performance. According to an experimental study, the main conclusions are follows below as listed:

- The adequate concentration for utilizing $Al_2O_3$- water nanofluid is equal to 0.3% as weight fraction.

- The cover glass cooling technology greatly improves the yield of hemispherical distillate.

- The cumulative yield of the modified distiller for utilizing $Al_2O_3$- water nanofluid with concentrations of 0.1, 0.2 and 0.3% improved by 41.8, 50.9, and 61.3%, respectively.

- Using the $Al_2O_3$- water nanofluid with concentrations of 0.1, 0.2 and 0.3%, and cooling of the glass cover, the productivity of the modified distiller increases by 105.8, 110.4, and 121%, respectively, compared the conventional distiller.

# General conclusion

In the current studies. First, the performance of the single slope solar still and hemispherical solar still was evaluated experimentally. The experiments were conducted continuously for 11 hours from 7 AM to 6 PM. Second, we were interested in using $Al_2O_3$- water nanofluid with three concentrations (0.1, 0.2 and 0.3%) and cooling of the glass cover with a constant water flow rate 0.008 kg/s to achieve the highest hemispherical distiller performance. According to experimental studies, and based on the obtained results, the main conclusions are follows below as listed:

- ✓ The results show that the hemispherical solar still gave 5.38 kg/m$^2$/day of yield for the duration of the experiment, whereas the single-slope solar distillery was given 3.64 kg/m$^2$/day.
- ✓ There is an improvement in the daily yield from the hemispherical solar still by 48% compared to the daily productivity of the single slope solar still.
- ✓ The daily accumulation of the hemispherical solar still has increased by 1.48 times, compared to the daily accumulation of the single-slope distillate.
- ✓ The maximum overall energy and exergy efficiencies were 38.6% and 3.1% for hemispherical solar still and 25.8% and 1.8% for the single slope solar still.
- ✓ We can recover the total cost of single slope solar still in 37 days, while of hemispherical solar still in 28 days, although total cost of hemispherical solar still is more expensive than single slope solar still.
- ✓ The adequate concentration for utilizing $Al_2O_3$- water nanofluid is equal to 0.3% as weight fraction.
- ✓ The cover glass cooling technology greatly improves the yield of hemispherical distillate.
- ✓ The cumulative yield of the modified distiller for utilizing $Al_2O_3$- water nanofluid with concentrations of 0.1, 0.2 and 0.3% improved by 41.8, 50.9, and 61.3%, respectively.
- ✓ Using the $Al_2O_3$- water nanofluid with concentrations of 0.1, 0.2 and 0.3%, and cooling of the glass cover, the productivity of the modified distiller increases by 105.8, 110.4, and 121%, respectively, compared the conventional distiller.

Finally, we recommend using a hemispherical solar distiller instead of using a single slope solar distiller. We also suggest strengthening the hemispherical distiller with nanoparticles to increase the heating of the basin water and cooling the transparent cover to increase the condensation process (to improve productivity).

We also suggest, as future studies, to enhance the absorbent of hemispherical solar distillates with metal trays, for example, on the one hand, and to cool the transparent cover on the other hand with a fan.

# Appendix A :

# Error analysis

# Appendix A: Error analysis

This section deals with the detailed description of error analysis of the instruments used during the experiment. Solar radiation, temperature and wind velocity are measured using solar power meter, PT100 RTD sensors and AM-4836 anemometer. Error of the instrument is defined as the ratio of least count of the instrument to the minimum value recorded.

## A.1. Solar power meter:

Make : TES 1333 Solar power meter

Range : 0-2500 $W/m^2$

Least count : 1 $W/m^2$

Minimum value recorded : 33 $W/m^2$

Error : 3.03 %

## A.2. Temperature:

Type : PT100 (RTD sensor)

Range : 0-100$^oC$

Least count : 0.1$^oC$

Minimum value recorded : 32$^oC$

Error : 0.31%

## A.3. Wind velocity:

Make : AM4836- 3 cup anemometer

Range : 0-45 m/s

Least count : 0.1 m/s

Minimum value recorded : 1 m/s

Error : 10 %

## A.4. Distillate collector:

Make : Borosil transparent graduated glass tube

Range : 0-1000 ml

Least count : 10 ml

Minimum value recorded : 200 ml

Error : 5 %

**Table (A.1):** Accuracy range and error of instruments used

| S.No | Instrument | Accuracy | Range | Error |
|---|---|---|---|---|
| 1 | TES 1333 Solar power meter | ± 1 $W/m^2$ | 0-2500 $W/m^2$ | 3.03 % |
| 2 | Thermocouple | ± 0.1°C | 0-100°c | 0.31 % |
| 3 | AM4836- 3 cup anemometer | ± 0.1 m/s | 0-45 m/s | 10 % |
| 4 | Distillate collector | ± 10 ml | 0-1000 ml | 5 % |

The mathematical expression for estimating the uncertainty is given as,

$$uncertainty = \frac{U}{X} \times 100 \qquad (A.1)$$

$$U = \frac{\sqrt{\sigma_1^2 + \sigma_2^2 + \sigma_3^2 \dots + \sigma_n^2}}{N} \qquad (A.2)$$

$$\sigma = \frac{\sqrt{\sum(X - \bar{X})}}{N} \qquad (A.3)$$

where

$X - \bar{X}$ Mean difference between observed value and average value.

N Number of observation.

**Table A.2 - A.4** shows the measured values of water, basin and glass temperature and the corresponding calculated uncertainty error. Similarly, the error of solar power meter is also measured with the available data as shown in **Table A.5**. The experimental error of solar power meter, water, basin and glass temperature are found to be 3.14, 1.26, 1.27 and 1.28% respectively.

**Table (A.2):** Evaluation of experimental uncertainty of water temperature

| Time | X | $(X-\bar{X})^2$ | X | $(X-\bar{X})^2$ | X | $(X-\bar{X})^2$ |
|---|---|---|---|---|---|---|
| 7 | 33 | 529 | 35 | 476.69 | 37 | 386.77 |
| 8 | 43 | 169 | 46 | 117.36 | 46 | 113.77 |
| 9 | 53 | 9 | 56 | 0.69 | 56 | 0.44 |
| 10 | 62 | 36 | 64 | 51.36 | 64 | 53.77 |
| 11 | 68 | 144 | 68 | 124.69 | 69 | 152.11 |
| 12 | 71 | 225 | 72 | 230.02 | 72 | 235.11 |
| 13 | 72 | 256 | 72 | 230.02 | 71 | 205.44 |
| 14 | 69 | 169 | 69 | 148.02 | 67 | 106.77 |
| 15 | 63 | 49 | 63 | 38.027 | 62 | 28.44 |
| 16 | 56 | 0 | 56 | 0.69 | 54 | 7.11 |
| 17 | 46 | 100 | 46 | 117.36 | 46 | 113.77 |
| 18 | 36 | 400 | 35 | 476.69 | 36 | 427.11 |
| Average and Sum | 56 | 2086 | 56.83 | 2011.66 | 56.66 | 1830.66 |
| | | | | | | |
| | | | | | | $\Sigma X=169.5$ |
| | | | | | | |
| $\sigma^2$ | 14.48 | | 13. 96 | | 12.71 | $\Sigma\sigma^2=41.16$ |
| % Uncertainty | | | | | | 1.26 |

**Table (A.3):** Evaluation of experimental uncertainty of basin temperature

| Time | X | $(X-\bar{X})^2$ | X | $(X-\bar{X})^2$ | X | $(X-\bar{X})^2$ |
|---|---|---|---|---|---|---|
| 7 | 33 | 532.84 | 36 | 437.51 | 37 | 410.06 |
| 8 | 44 | 146.01 | 46 | 119.17 | 47 | 105.06 |
| 9 | 54 | 4.34 | 56 | 0.84 | 57 | 0.06 |
| 10 | 62 | 35.01 | 64 | 50.17 | 64 | 45.56 |
| 11 | 68 | 142.01 | 69 | 146.01 | 70 | 162.56 |
| 12 | 71 | 222.51 | 72 | 227.51 | 72 | 217.56 |
| 13 | 72 | 253.34 | 73 | 258.67 | 72 | 217.56 |
| 14 | 68 | 142.01 | 70 | 171.17 | 69 | 138.06 |
| 15 | 63 | 47.84 | 63 | 37.01 | 63 | 33.06 |
| 16 | 56 | 0.01 | 56 | 0.84 | 55 | 5.06 |
| 17 | 46 | 101.67 | 44 | 166.84 | 46 | 126.56 |
| 18 | 36 | 403.34 | 34 | 525.17 | 35 | 495.06 |
| Average and Sum | 56.08 | 2030.92 | 56.92 | 2140.92 | 57.25 | 1956.25 |
| | | | | | | |
| | | | | | | ΣX=170.25 |
| | | | | | | |
| $\sigma^2$ | 14.10 | | 14.87 | | 13.59 | $\Sigma\sigma^2$=42.56 |
| % Uncertainty | | | | | | 1.28 |

**Table (A.4):** Evaluation of experimental uncertainty of glass temperature

| Time | X | $(X-\bar{X})^2$ | X | $(X-\bar{X})^2$ | X | $(X-\bar{X})^2$ |
|---|---|---|---|---|---|---|
| 7 | 32 | 502.51 | 34 | 390.06 | 32 | 255.11 |
| 8 | 43 | 130.34 | 43 | 115.56 | 39 | 205.44 |
| 9 | 52 | 5.84 | 53 | 0.56 | 49 | 18.78 |
| 10 | 60 | 31.17 | 58 | 18.06 | 58 | 21.78 |
| 11 | 60 | 134.17 | 65 | 126.56 | 65 | 136.11 |
| 12 | 70 | 242.84 | 68 | 203.06 | 68 | 215.11 |
| 13 | 70 | 242.84 | 68 | 203.06 | 69 | 245.44 |
| 14 | 67 | 158.34 | 65 | 126.56 | 67 | 186.78 |
| 15 | 61 | 43.34 | 60 | 39.06 | 61 | 58.78 |
| 16 | 53 | 2.01 | 52 | 3.06 | 53 | 0.11 |
| 17 | 44 | 108.51 | 44 | 95.06 | 44 | 87.11 |
| 18 | 35 | 377.01 | 35 | 351.56 | 35 | 336.11 |
| Average and Sum | 54.42 | 1978.92 | 53.75 | 1672.25 | 53.33 | 1966.67 |
| | | | | | | |
| | | | | | | $\Sigma X=161.5$ |
| | | | | | | |
| $\sigma^2$ | 13.37 | | 11.61 | | 13.66 | $\Sigma\sigma^2=39.01$ |
| % Uncertainty | | | | | | 1.29 |

**Table (A.5):** Evaluation of experimental uncertainty of solar power meter

| Time | X | $(X-\bar{X})^2$ | X | $(X-\bar{X})^2$ | X | $(X-\bar{X})^2$ |
|---|---|---|---|---|---|---|
| 7 | 1 | 279708.6 | 5.3 | 337134.1 | 50.4 | 351065.4 |
| 8 | 218.9 | 96716.4 | 241.6 | 118576.5 | 314.1 | 108130.3 |
| 9 | 461.8 | 4627.6 | 497 | 7907.4 | 572.7 | 4928.9 |
| 10 | 668.8 | 19297.6 | 716.2 | 16974.3 | 791.8 | 22168.6 |
| 11 | 820.2 | 84321.1 | 879 | 85899.7 | 952.1 | 95631.5 |
| 12 | 903.6 | 139647.3 | 971.9 | 149008.8 | 1040.8 | 158301.8 |
| 13 | 912.0 | 14601.6 | 987.6 | 161342.5 | 1050.7 | 166312.3 |
| 14 | 845.0 | 99280.5 | 924.8 | 114804.7 | 981.2 | 114444.6 |
| 15 | 707.7 | 31637.6 | 788.4 | 40985.3 | 837.6 | 37930.2 |
| 16 | 511.7 | 329.7 | 589.5 | 12.9 | 631.6 | 127.9 |
| 17 | 274.6 | 65159.0 | 345.5 | 57815.3 | 380.5 | 68828.3 |
| 18 | 33.1 | 246799.3 | 84.4 | 251584.2 | 111.2 | 282670.7 |
| Average and Sum | 529.86 | 1213566 | 585.93 | 1342046 | 642.88 | 1410540 |
| | | | | | | |
| | | | | | | $\Sigma X=1758.68$ |
| | | | | | | |
| $\sigma^2$ | 8427.54 | | 9319.76 | | 9795.41 | $\Sigma\sigma^2=27542.73$ |
| % Uncertainty | | | | | | 3.14 |

# Appendix B :

# Experimental results

# Appendix B: Experimental results

**Table (B.1):** Calculated and measured hour parameters for MHSSN-1 and MHSSNS-1 hemispherical distillers as of 25/09/2020

| 25-09-2020 | Ta (°C) | Solar Wh/m$^2$ | Cooling water temperature(°C) | Water basin temperature (°C) | | | Internal glass temperature (°C) | | | External glass temperature (°C) | | | Product water (ml) | | |
|---|---|---|---|---|---|---|---|---|---|---|---|---|---|---|---|
| | | | | CHSS | MHSSN-1 | MHSSNC-1+Cooling | CHSS | MHSSN-1 | MHSSNC-1+Cooling | CHSS | MHSSN-1 | MHSSNC-1+Cooling | CHSS | MHSSN-1 | MHSSNC-1+Cooling |
| 08:00 | 30 | 381 | 27 | 31 | 31 | 31 | 30 | 30 | 27 | 30 | 30 | 28 | 0 | 0 | 0 |
| 09:00 | 32 | 634 | 28 | 39 | 40 | 41 | 33 | 32 | 28 | 31 | 31 | 28 | 3 | 5 | 10 |
| 10:00 | 38 | 841 | 37 | 46 | 49 | 50 | 43 | 44 | 39 | 40 | 40 | 37 | 25 | 35 | 60 |
| 11:00 | 43 | 967 | 40 | 52 | 54 | 53 | 49 | 49 | 45 | 46 | 46 | 41 | 35 | 45 | 75 |
| 12:00 | 46 | 1006 | 44 | 56 | 59 | 59 | 53 | 53 | 47 | 50 | 50 | 46 | 40 | 60 | 85 |
| 13:00 | 47 | 967 | 46 | 57 | 61 | 61 | 53 | 53 | 48 | 50 | 50 | 47 | 45 | 65 | 90 |
| 14:00 | 48 | 841 | 46 | 60 | 63 | 62 | 53 | 53 | 47 | 50 | 50 | 48 | 45 | 65 | 85 |
| 15:00 | 48 | 634 | 46 | 60 | 62 | 61 | 53 | 54 | 47 | 50 | 50 | 47 | 45 | 60 | 80 |
| 16:00 | 44 | 381 | 44 | 57 | 60 | 60 | 51 | 51 | 46 | 48 | 48 | 45 | 40 | 55 | 75 |
| 17:00 | 42 | 139 | 42 | 57 | 59 | 58 | 49 | 49 | 45 | 46 | 46 | 43 | 30 | 40 | 65 |
| 18:00 | 38 | 23 | 38 | 52 | 55 | 56 | 45 | 45 | 42 | 42 | 42 | 39 | 20 | 35 | 50 |
| | | | | | | | | | | | | | 328 | 465 | 675 |

**Table (B.2):** Calculated and measured hour parameters for MHSSN-2 and MHSSNS-2 hemispherical distillers as of 26/09/2020

| 26-09-2020 | Ta (°C) | Solar $Wh/m^2$ | Cooling water temperature(°C) | Water basin temperature (°C) | | | Internal glass temperature (°C) | | | External glass temperature (°C) | | | Product water (ml) | | |
|---|---|---|---|---|---|---|---|---|---|---|---|---|---|---|---|
| | | | | CHSS | MHSSN-2 | MHSSNC-2+Cooling | CHSS | MHSSN-2 | MHSSNC-2+Cooling | CHSS | MHSSN-2 | MHSSNC-2+Cooling | CHSS | MHSSN-2 | MHSSNC-2+Cooling |
| 08:00 | 30 | 380 | 27 | 30 | 30 | 30 | 29 | 29 | 29 | 29 | 29 | 27 | 0 | 0 | 0 |
| 09:00 | 33 | 634 | 28 | 39 | 42 | 41 | 33 | 33 | 29 | 31 | 31 | 28 | 3 | 5 | 10 |
| 10:00 | 36 | 841 | 32 | 47 | 50 | 50 | 43 | 43 | 38 | 39 | 39 | 34 | 22 | 35 | 65 |
| 11:00 | 42 | 967 | 37 | 52 | 58 | 58 | 48 | 48 | 44 | 46 | 46 | 40 | 35 | 50 | 75 |
| 12:00 | 46 | 1006 | 44 | 56 | 62 | 63 | 53 | 53 | 48 | 50 | 50 | 44 | 40 | 60 | 85 |
| 13:00 | 46 | 967 | 46 | 59 | 63 | 63 | 53 | 53 | 50 | 50 | 50 | 45 | 50 | 70 | 90 |
| 14:00 | 45 | 841 | 46 | 60 | 64 | 65 | 53 | 53 | 50 | 50 | 50 | 46 | 45 | 70 | 90 |
| 15:00 | 45 | 634 | 47 | 58 | 64 | 63 | 54 | 54 | 51 | 50 | 50 | 45 | 40 | 65 | 80 |
| 16:00 | 44 | 380 | 46 | 57 | 62 | 62 | 52 | 52 | 49 | 49 | 49 | 44 | 35 | 55 | 75 |
| 17:00 | 42 | 138 | 44 | 56 | 61 | 60 | 50 | 50 | 47 | 46 | 46 | 43 | 30 | 45 | 65 |
| 18:00 | 42 | 24 | 42 | 51 | 58 | 59 | 48 | 48 | 44 | 44 | 44 | 41 | 25 | 40 | 55 |
| | | | | | | | | | | | | | 325 | 495 | 690 |

**Table (B.3):** Calculated and measured hour parameters for MHSSN-3 and MHSSNS-3 hemispherical distillers as of 27/09/2020

| 27-09-2020 | Ta (°C) | Solar Wh/m 2 | Cooling water temperature(°C) | Water basin temperature (°C) | | | Internal glass temperature (°C) | | | External glass temperature (°C) | | | Product water (ml) | | |
|---|---|---|---|---|---|---|---|---|---|---|---|---|---|---|---|
| | | | | CHSS | MHSSN -3 | MHSSNC-3+Cooling | CHS S | MHSSNC -3 | MHSSNC-3+Cooling | CHS S | MHSSNC -3 | MHSSNC-3+Cooling | CHS S | MHSSN -3 | MHSSN C-3+Cooli ng |
| 08:00 | 30 | 378 | 27 | 30 | 30 | 30 | 29 | 29 | 28 | 29 | 29 | 27 | 0 | 0 | 0 |
| 09:00 | 33 | 633 | 28 | 38 | 44 | 45 | 34 | 34 | 30 | 30 | 30 | 28 | 2 | 5 | 10 |
| 10:00 | 36 | 841 | 33 | 48 | 53 | 52 | 40 | 40 | 36 | 38 | 38 | 34 | 25 | 35 | 67 |
| 11:00 | 40 | 968 | 39 | 51 | 60 | 61 | 47 | 48 | 43 | 41 | 41 | 38 | 37 | 55 | 78 |
| 12:00 | 42 | 1007 | 40 | 56 | 64 | 63 | 50 | 50 | 46 | 47 | 47 | 40 | 40 | 70 | 90 |
| 13:00 | 44 | 968 | 40 | 58 | 65 | 64 | 52 | 52 | 48 | 50 | 50 | 45 | 50 | 72 | 95 |
| 14:00 | 46 | 841 | 42 | 60 | 66 | 66 | 55 | 55 | 51 | 50 | 50 | 46 | 45 | 75 | 95 |
| 15:00 | 45 | 633 | 43 | 59 | 66 | 66 | 53 | 53 | 49 | 50 | 50 | 44 | 40 | 70 | 85 |
| 16:00 | 43 | 378 | 41 | 58 | 64 | 65 | 51 | 51 | 47 | 48 | 48 | 43 | 35 | 60 | 80 |
| 17:00 | 42 | 137 | 40 | 55 | 63 | 62 | 50 | 50 | 46 | 46 | 46 | 42 | 30 | 45 | 65 |
| 18:00 | 41 | 22 | 40 | 51 | 60 | 61 | 49 | 49 | 45 | 44 | 44 | 41 | 25 | 40 | 60 |
| | | | | | | | | | | | | | 329 | 527 | 725 |

**Table (B.4):** Abbreviations

| | |
|---|---|
| CHSS | Conventional Hemispherical Solar Still |
| MHSSN-1 | Modified Hemispherical Solar Still with 0.1% Nanoparticles of $Al_2O_3$ |
| MHSSN-2 | Modified Hemispherical Solar Still with 0.2% Nanoparticles of $Al_2O_3$ |
| MHSSN-3 | Modified Hemispherical Solar Still with 0.3% Nanoparticles of $Al_2O_3$ |
| MHSSNS-1 | Modified Hemispherical Solar Still with 0.1% Nanoparticles of $Al_2O_3$ and water Sprinkler (0.008 Kg/s) |
| MHSSNS-2 | Modified Hemispherical Solar Still with 0.2% Nanoparticles of $Al_2O_3$ and water Sprinkler (0.008 Kg/s) |
| MHSSNS-3 | Modified Hemispherical Solar Still with 0.3% Nanoparticles of $Al_2O_3$ and water Sprinkler (0.008 Kg/s) |

# References

# References

Aburideh, H., Deliou, A., Abbad, B., Alaoui, F., Tassalit, D., & Tigrine, Z. (2012). An experimental study of a solar still: Application on the sea water desalination of Fouka. Procedia Engineering, 33, 475-484. https://doi.org/10.1016/j.proeng.2012.01.1227.

Ahsan, A., Imteaz, M., Rahman, A., Yusuf, B., & Fukuhara, T. (2012). Design, fabrication and performance analysis of an improved solar still. Desalination, 292, 105-112. https://doi.org/10.1016/j.desal.2012.02.013.

Ali, G. A., Fouad, O. A., & Makhlouf, S. A. (2013). Structural, optical and electrical properties of sol–gel prepared mesoporous $Co_3O_4/SiO_2$ nanocomposites. Journal of alloys and compounds, 579, 606-611. https://doi.org/10.1016/j.jallcom.2013.07.095.

Arunkumar, T., Jayaprakash, R., & Ahsan, A. (2012). A comparative experimental testing in enhancement of the efficiency of pyramid solar still and hemispherical solar still. Journal of Renewable Energy and Smart Grid Technology, 7(2), 1-8. https://ph01.tci-thaijo.org/index.php/RAST/article/view/26223.

Arunkumar, T., Jayaprakash, R., Denkenberger, D., Ahsan, A., Okundamiya, M. S., Tanaka, H., & Aybar, H. Ş. (2012a). An experimental study on a hemispherical solar still. Desalination, 286, 342-348. https://doi.org/10.1016/j.desal.2011.11.047.

Ashtiani, S., & Hormozi, F. (2020). Design improvement in a stepped solar still based on entropy generation minimization. Journal of Thermal Analysis and Calorimetry, 140(3), 1095-1106. https://doi.org/10.1007/s10973-019-08580-3.

Attia, M. E. H., Abdelgaied, M., El-Maghlany, W. M., & Driss, Z. (2021). Enhancement of the performance of hemispherical distiller via phosphate pellets as energy storage medium. Environmental Science and Pollution Research, 28, 32386–32395. https://doi.org/10.1007/s11356-021-12920-y.

Attia, M. E. H., Hussein, A. K., Rout, S. K., Soli, J., Elaloui, E., Driss, Z., & Chand, R. (2021). Experimental Study of the Effect of $Al_2O_3$ Nanoparticles on the

# References

Profitability of a Single-Slope Solar Still: Application in Southeast of Algeria. In Advances in Air Conditioning and Refrigeration. Springer Singapore, 119-133. https://doi.org/10.1007/978-981-15-6360-7_12.

Attia, M. E. H., Kabeel, A. E., Abdelgaied, M., & Driss, Z. (2020). Productivity enhancement of traditional solar still by using sandbags of El Oued, Algeria. Heat Transfer, 50(1), 768-783. https://doi.org/10.1002/htj.783.

Attia, M. E. H., Karthick, A., Manokar, A. M., Driss, Z., Sathyamurthy, R., & Sharifpur, M. (2020a). Sustainable potable water production from conventional solar still during the winter season at Algerian dry areas: energy and exergy analysis. Journal of Thermal Analysis and Calorimetry, 1-11. https://doi.org/10.1016/j.desal.2011.04.042.

Attia, M. E. H., Karthick, A., Manokar, A. M., Driss, Z., Kabeel, A. E., Sathyamurthy, R., & Sharifpur, M. (2020b). Sustainable potable water production from conventional solar still during the winter season at Algerian dry areas: energy and exergy analysis. J Therm Anal Calorim, 145, 1215-1225 https://doi.org/10.1007/s10973-020-10277-x.

Attia, M. E. H., Driss, Z., Abdelgaied, M., Manokar, A. M., Sathyamurthy, R., & Hussein, A. K. (2020c). Performance evaluation of modified solar still using aluminum foil sheet as absorber cover–a comparative study. Journal of Testing and Evaluation, 49(5). https://doi.org/10.1520/JTE20200249.

Attia, M.E.H., Kabeel, A.E, Abdelgaied, M., Bellila, A. (2022a). Optimization of the hemispherical solar distiller performance assisted by high thermal conductivity metal trays incorporated with reflective mirrors. Environmental Science and Pollution Research. Vol.:(0112 33456789). https://doi.org/10.1007/s11356-022-18708-y.

Attia, M. E. H., Kabeel, A. E., Abdelgaied, M., Moataz, M. A. E.A. , Bellila, A., & Abdelkader., A. (2021d). Optimal size of black gravel as energy storage materials for performance improvement of hemispherical distillers. Journal of Energy Storage, vol 43, https://doi.org/10.1016/j.est.2021.103196.

Attia, M. E. H., Kabeel, A. E., Abdelgaied, M., Bellila, A., & Moataz, M. A. E.A. (2021c). Optimal concentration of high thermal conductivity sensible storage materials (graphite) for performance enhancement of hemispherical distillers. Desalination and Water Treatment, vol https://doi.org/10.1016/j.est.2021.102415.

Attia, M. E. H., Kabeel, A. E., Abdelgaied, M., El-Maghlany, W. M., & Bellila, A. (2021a). Comparative study of hemispherical solar distillers iron-fins. Journal of Cleaner Production, vol292, https://doi.org/10.1016/j.jclepro.2021.126071.

Attia, M. E. H., Kabeel, A. E., Bellila, A., El-Maghlany, W. M., Abdelgaied, M., El-Agouz, S. A., & Abdel-Aziz, M. M. (2022c). Enhancing hemispherical solar still yield via wick materials and glass cover cooling. DESALINATION AND WATER TREATMENT, 247, 1-9. https:// doi.org/ 10.5004/dwt.2022.28049.

Attia, M. E. H., Kabeel, A. E., Bellila, A., Manokar, A. M., Sathyamurthy, R., Driss, Z., & Muthusamy, S. (2021b). A comparative energy and exergy efficiency study of hemispherical and single-slope solar stills. *Environmental Science and Pollution Research*, *28*(27), 35649-35659. https://doi.org/10.1007/s11356-021-13161-9.

M. E. H. Attia., Kabeel, A. E., Ahmed, A., Abdelgaied, M., Bellila, A., & Abdullah, A.S. (2022d). Optimal configurations of hemispherical solar distillers using the higher conductivity extended hollow cylindrical fins filled with latent heat storage materials. Journal of Energy Storage. 50. 104706. https://doi.org/10.1016/j.est.2022.104706.

M. E. H. Attia., W. M. El-Maghlany., A. E. Kabeel., M. Abdelgaied., & A. Bellila. (2022b). Technically and economically optimal water flow rate glass film cooling for hemispherical drinking water distillers. International Journal of Environmental Science and Technology. https://doi.org/10.1007/s13762-021-03859-1.

Bellila, A., Attia, M. E. H., Kabeel, A. E., Abdelgaied, M., Harby, K., & Soli, J. (2021). Productivity enhancement of hemispherical solar still using Al2O3-water-based nanofluid and cooling the glass cover. *Applied Nanoscience*, *11*(4), 1127- 1139. https://doi.org/10.1007/s13204-021-01677-y.

Chaichan, M. T., & Kazem, H. A. (2015). Water solar distiller productivity enhancement using concentrating solar water heater and phase change material

(PCM). Case studies in thermal engineering, 5, 151-159. https://doi.org/10.1016/j.csite.2015.03.009.

Chaichan, M. T., & Kazem, H. A. (2018). Single slope solar distillator productivity improvement using phase change material and $Al_2O_3$ nanoparticle. Solar Energy, 164, 370-381. https://doi.org/10.1016/j.solener.2018.02.049.

Chaichan, M. T., Abaas, K. I., & Kazem, H. A. (2016). Design and assessment of solar concentrator distillating system using phase change materials (PCM) suitable for desertic weathers. Desalination and water treatment, 57(32), 14897-14907. https://doi.org/10.1080/19443994.2015.1069221.

Dev, R., & Tiwari, G. N. (2009). Characteristic equation of a passive solar still. Desalination, 245 (1-3), 246–265. https://doi.org/10.1016/j.desal.2008.07.011.

El Mir, L., Amlouk, A., Elaloui, E., Saadoun, M., & Pierre, A. C. (2008). Preparation and optical characterization of transparent, microporous TiO2 xerogel monoliths. Materials Science and Engineering: B, 146(1-3), 69-73. https://doi.org/10.1016/j.mseb.2007.07.055.

El-Agouz, S. A., El-Samadony, Y. A. F., & Kabeel, A. E. (2015). Performance evaluation of a continuous flow inclined solar still desalination system. Energy Conversion and Management, 101, 606-615. https://doi.org/10.1016/j.enconman.2015.05.069.

Elaloui, E., & Pajonk; G. M. (2000). Synthèse sol-gel : application à la silice. J Société Chimique Tunisie, 4, 607.

Elaloui, E., Begag, R., Pommier, B., & Pajonk, G. M. (2002). Thermos table yttria doped inorganic oxide catalyst supports for high temperature reactions. Stud Surf Sci Catal, 143, 331.

Elaloui, E., Pierre, A. C., & Pajonk, G. M. (1997). Influence of the sol-gel processing method on the structure and the porous texture of nondoped aluminas. Journal of Catalysis, 166(2), 340-346. https://doi.org/10.1006/jcat.1997.1540.

Elango, T., Kannan, A., & Murugavel, K. K. (2015). Performance study on single basin single slope solar still with different water nanofluids. Desalination, 360, 45-51. https://doi.org/10.1016/j.desal.2015.01.004.

# References


Elghniji, K., Ksibi, M., & Elaloui, E. (2012). Sol–gel reverse micelle preparation and characterization of N-doped $TiO_2$: efficient photo catalytic degradation of methylene blue in water under visible light. J Ind Eng Chem, 18, 178 . https://doi.org/10.1016/j.jiec.2011.11.011.

Farahmandjou, M., & Motaghi, S. (2019). Sol–gel synthesis of Ce-doped α-$Al_2O_3$: study of crystal and optoelectronic properties. Optics Communications, 441, 1-7. https://doi.org/10.1016/j.optcom.2019.02.029.

Fouad, O. A., Makhlouf, S. A., Ali, G. A., & El-Sayed, A. Y. (2011). Cobalt/silica nanocomposite via thermal calcination-reduction of gel precursors. Materials Chemistry and Physics, 128(1-2), 70-76. https://doi.org/10.1016/j.matchemphys.2011.02.072.

Gaur, M. K., & Tiwari, G. N. (2010). Optimization of number of collectors for integrated PV/T hybrid active solar still. Appl Energy, 87(5), 1763–1772. https://doi.org/10.1016/j.apenergy.2009.10.019.

Gupta, B., Shankar, P., Sharma, R., & Baredar, P. (2016). Performance enhancement using nano particles in modified passive solar still. Procedia Technology, 25, 1209-1216. https://doi.org/10.1016/j.protcy.2016.08.208.

Hansen, R. S., Narayanan, C. S., & Murugavel, K. K. (2015). Performance analysis on inclined solar still with different new wick materials and wire mesh. Desalination, 358, 1-8. https://doi.org/10.1016/j.desal.2014.12.006.

Hu, B., Jia, E., Du, B., & Yin, Y. (2016). A new sol-gel route to prepare dense $Al_2O_3$ thin films. Ceram Int, 42, 16867–16871. https://doi.org/10.1016/j.ceramint.2016.07.181.

Ismail, B. I. (2009). Design and performance of a transportable hemispherical solar still. Renewable Energy, 34(1), 145-150. https://doi.org/10.1016/j.renene.2008.03.013.

Jayaprakash, R., Arunkumar, T., & Kumar, S. (2012). Parametric modelling and experimental evaluation of hemispherical solar still for fresh water production. Journal of Renewable Energy and Smart Grid Technology, 7(1), 43-62. https://ph01.tci-thaijo.org/index.php/RAST/article/view/26217.

# References

Kabeel, A. E. (2009). Performance of solar still with a concave wick evaporation surface, Energy Elsevier, 34(10), 1504-1509. https://doi.org/10.1016/j.energy.2009.06.050.

Kabeel, A. E., Teamah, M. A, Abdelgaied, M., & Aziz, G. B. A. (2017). Modified pyramid solar still with v-corrugated absorber plate and PCM as a thermal storage medium, J. Cleaner Prod., 161, 881–887. https://doi.org/10.1016/j.jclepro.2017.05.195.

Kabeel, A. E., & Abdelgaied, M. (2017a). Observational study of modified solar still coupled with oil serpentine loop from cylindrical parabolic concentrator and phase changing material under basin, Sol. Energy, 144, 71–78. https://doi.org/10.1016/j.solener.2017.01.007.

Kabeel, A. E., & Abdelgaied, M. (2017b). Performance enhancement of modified solar still using multi-groups of two coaxial pipes in basin. Applied Thermal Engineering, 118, 23-32. https://doi.org/10.1016/j.applthermaleng.2017.02.090.

Kabeel, A. E., & Abdelgaied, M. (2019). Performance enhancement of a photovoltaic panel with reflectors and cooling coupled to a solar still with air injection. J. Clean. Prod, 224, 40-49. https://doi.org/10.1016/j.jclepro.2019.03.199.

Kabeel, A. E., Sharshir, S. W., Abdelaziz, G. B., Halim, M. A., & Swidan, A. (2019a). Improving performance of tubular solar still by controlling the water depth and cover cooling. Journal of cleaner production, 233, 848-856. https://doi.org/10.1016/j.jclepro.2019.06.104.

Kabeel, A. E., Abdelgaied, M., & Eisa., A. (2019b). Effect of graphite mass concentrations in a mixture of graphite nanoparticles and paraffin wax as hybrid storage materials on performances of solar still. Renew Energy, 132, 119–128. https://doi.org/10.1016/j.renene.2018.07.147.

Kabeel, A. E., Abdelgaied, M., & Eisa, A. (2018). Enhancing the performance of single basin solar still using high thermal conductivity sensible storage materials. Journal of cleaner production, 183, 20-25. https://doi.org/10.1016/j.jclepro.2018.02.144.

# References

Kabeel, A. E., Abdelgaied, M., & Mahmoud, G. M. (2021). Performance evaluation of continuous solar still water desalination system. Journal of Thermal Analysis & Calorimetry, 144(3). https://doi.org/10.1007/s10973-020-09547-5.

Kabeel, A. E., Harby, K., Abdelgaied, M., & Eisa, A. (2020). A comprehensive review of tubular solar still designs, performance, and economic analysis. Journal of Cleaner Production, 246, 119030. https://doi.org/10.1016/j.jclepro.2019.119030.

Kabeel, A. E., Omara, Z. M., & Essa, F. A. (2014). Enhancement of modified solar still integrated with external condenser using nanofluids: An experimental approach. Energy conversion and management, 78, 493-498. https://doi.org/10.1016/j.enconman.2013.11.013.

Kabeel, A. E., Omara, Z. M., & Essa, F. A. (2014a). Improving the performance of solar still by using nanofluids and providing vacuum. Energy conversion and management, 86, 268-274. https://doi.org/10.1016/j.enconman.2014.05.050.

Kachbouri, S., Elaloui, E., & Moussaoui, Y. (2019). The effect of surfactant chain length and type on the photo catalytic activity of mesoporous $TiO_2$ nanoparticles obtained via modified Sol-Gel process. Iran J Chem Chem Eng, 38(1), 17–26. https://doi.org/10.30492/IJCCE.2019.29528.

Katekar, V. P., & Deshmukh, S. S. (2020). A review on research trends in solar still designs for domestic and industrial applications. Journal of Cleaner Production, 257, 120544. https://doi.org/10.1016/j.jclepro.2020.120544.

Khechekhouche, A., Kabeel, A. E., Benhaoua, B., Attia, M. E. H., & El-said, E. (2020). Traditional solar distiller improvement by a single external refractor under the climatic conditions of the El-Oued region, Algeria. Desalin Water Treat, 177, 23-28. https: //doi: 10.5004/dwt.2020.24832.

Kumar, B. S., Kumar, S., & Jayaprakash, R. (2008). Performance analysis of a “V” type solar still using a charcoal absorber and a boosting mirror. Desalination, 229(1-3), 217-230. https://doi.org/10.1016/j.desal.2007.09.009.

Kumar, S., & Tiwari, A. (2010). Design, fabrication and performance of a hybrid photovoltaic/thermal (PV/T) active solar still. Energy Conversion and Management, 51(6), 1219-1229. https://doi.org/10.1016/j.enconman.2009.12.033.

# References

Manokar, A. M., Vimala, M., Sathyamurthy, R., Kabeel, A. E., Winston, D. P., & Chamkha, A. J. (2020). Enhancement of potable water production from an inclined photovoltaic panel absorber solar still by integrating with flat-plate collector. Environ Dev Sustain, 22(5), 4145–4167. https://doi.org/10.1007/s10668-019-00376-7.

Manokar, A. M., Winston, D. P., Mondol, J. D., Sathyamurthy, R., Kabeel, A. E., & Panchal, H. (2018). Comparative study of an inclined solar panel basin solar still in passive and activemode. Sol Energy, 169, 206–216. https://doi.org/10.1016/j.solener.2018.04.060.

Manokar, A. M., Winston, D. P., Sathyamurthy, R., Kabeel, A. E., & Prasath, A. R. (2019). Experimental investigation on pyramid solar still in passive and active mode. Heat Mass Transf, 55(4), 1045–1058. https://doi.org/10.1007/s00231-018-2483-3.

Modi, K. V., & Shukla, D. L. (2018). Regeneration of liquid desiccant for solar air-conditioning and desalination using hybrid solar still. Energy Conser Manage, 171, 1598–1616. https://doi.org/10.1016/j.enconman.2018.06.096.

Murugavel, K. K., & Srithar, K. (2011). Performance study on basin type double slope solar still with different wick materials and minimum mass of water. Renew Energy, 36(2), 612–620. https://doi.org/10.1016/j.renene.2010.08.009.

Nazari, S., Safarzadeh, H., & Bahiraei, M. (2019). Performance improvement of a single slope solar still by employing thermoelectric cooling channel and copper oxide nanofluid: an experimental study. J Cleaner Prod, 208(20), 1041–1052. https://doi.org/10.1016/j.jclepro.2018.10.194.

Nijmeh, S., Odeh, S., & Akash, B. (2005). Experimental and theoretical study of a single-basin solar sill in Jordan. International communications in heat and mass transfer, 32(3-4), 565-572. https://doi.org/10.1016/j.icheatmasstransfer.2004.06.006.

Omara, Z. M., Kabeel, A. E., & Essa, F. A. (2015). Effect of using nanofluids and providing vacuum on the yield of corrugated wick solar still. Energy conversion and management, 103, 965-972. https://doi.org/10.1016/j.enconman.2015.07.035.

Pajonk, G. M., Rao, A. V., Parvathy, N. N., & Elaloui, E. (1996). Microstructural characterization of silica aerogels using scanning electron microscopy. Journal of materials science, 31(21), 5683-5689. https://doi.org/10.1007/BF01160815.

Patel, S. K., & Modi, K. V. (2020). Techniques to improve the performance of enhanced condensation area solar still: A critical review. Journal of Cleaner Production, 268, 122260. https://doi.org/10.1016/j.jclepro.2020.122260.

Peng, Y., Nie, J., Zhang, W., Ma, J., Bao, C., & Cao, Y. (2016). Effect of the addition of $Al_2O_3$ nanoparticles on the magnetic properties of Fe soft magnetic composites. J Magn, 399, 88–93. https://doi.org/10.1016/j.jmmm.2015.09.069.

Phadatare, M. K., & Verma, S. K. (2007). Influence of water depth on internal heat and mass transfer in a plastic solar still. Desalination, 217(1-3), 267-275. https://doi.org/10.1016/j.desal.2007.03.006.

Ponthieu, E., Grimblot, J., Elaloui, E., & Pajonk, G. M. (1993). Synthesis and characterization of pure and yttrium-containing alumina aerogels. Journal of materials chemistry, 3(3), 287-293. https://doi.org/10.1039/JM9930300279

Rajamanickam, M. R., & Ragupathy, A. (2012). Influence of water depth on internal heat and mass transfer in a double slope solar still. Energy procedia, 14, 1701-1708. https://doi.org/10.1016/j.egypro.2011.12.1155.

Sahota, L., & Tiwari, G. N. (2016). Effect of $Al_2O_3$ nanoparticles on the performance of passive double slope solar still. Solar Energy, 130, 260-272. https://doi.org/10.1016/j.solener.2016.02.018.

Sakthivel, T. G., & Arjunan, T. V. (2019). Thermodynamic performance comparison of single slope solar stills with and without cotton cloth energy storage medium. Journal of Thermal Analysis and Calorimetry, 137(1), 351-360. https://doi.org/10.1007/s10973-018-7909-0.

Samee, M. A., Mirza, U. K., Majeed, T., & Ahmad, N. (2007). Design and performance of a simple single basin solar still. Renewable and Sustainable Energy Reviews, 11(3), 543-549. https://doi.org/10.1016/j.rser.2005.03.003.

Shanmugan, S., Palani, S., & Janarthanan, B. (2018). Productivity enhancement of solar still by PCM and Nanoparticles miscellaneous basin absorbing materials. Desalination, 433, 186-198. https://doi.org/10.1016/j.desal.2017.11.045.

## References

Sharshir, S. W., Ellakany, Y. M., & Eltawil, M. A. (2020). Exergoeconomic and environmental analysis of seawater desalination system augmented with nanoparticles and cotton hung pad. Journal of Cleaner Production, 248, 119180. https://doi.org/10.1016/j.jclepro.2019.119180.

Somanchi, N. S., Sagi, S. L. S., Kumar, T. A., Kakarlamudi, S. P. D., & Parik, A. (2015). Modelling and analysis of single slope solar still at different water depth. Aquatic procedia, 4, 1477-1482. https://doi.org/10.1016/j.aqpro.2015.02.191.

Subhedar, D. G., Chauhan, K. V., Patel, K., & Ramani, B. M. (2020). Performance improvement of a conventional single slope single basin passive solar still by integrating with nanofluid-based parabolic trough collector: an experimental study. Today Proc, 26(2), 1478–1481. https://doi.org/10.1016/j.matpr.2020.02.304.

Suneesh, P. U., Jayaprakash, R., Arunkumar, T., & Denkenberger, D. (2014). Effect of air flow on "V" type solar still with cotton gauze cooling. Desalination, 337, 1–5. https://doi.org/10.1016/j.desal.2013.12.035.

Taamneh, Y., & Taamneh, M. M. (2012). Performance of pyramid-shaped solar still: Experimental study. Desalination, 291, 65-68. https://doi.org/10.1016/j.desal.2012.01.026.

Tabesh, S., Davar, F., & Loghman-estarki, M. R. (2018) Preparation of γ-$Al_2O_3$ nanoparticles using modified sol-gel method and its use for the adsorption of lead and cadmium ions. J Alloys Compd, 730, 441–449. https://doi.org/10.1016/j.jallcom.2017.09.246.

Tangsir, S., Hafshejani, L. D., Lähde, A., Maljanen, M., Hooshmand, A., Naseri, A. A., & Bhatnagar, A. (2016). Water defluoridation using $Al_2O_3$ nanoparticles synthesized by flame spray pyrolysis (FSP) method. Chemical Engineering Journal, 288, 198-206. https://doi.org/10.1016/j.cej.2015.11.097.

Tiwari, G. N., & Kumar, A. (1988). Nocturnal water production by tubular solar stills using waste heat to preheat brine. Desalination, 69(3), 309-318. https://doi.org/10.1016/0011-9164(88)80032-8.

Vaithilingam, S., & Esakkimuthu, G. S. (2015). Energy and exergy analysis of single slope passive solar still: an experimental investigation. Desalination and Water Treatment, 55(6), 1433-1444. https://doi.org/10.1080/19443994.2014.928794.

# References

Zhang, L., Wu, Y., Zhang, L., Wang, Y., & Li, M. (2016). Synthesis and characterization of mesoporous alumina with high specific area via coprecipitation method. Vacuum, 133, 1-6. https://doi.org/10.1016/j.vacuum.2016.08.005.

**Abstract:** This thesis is divided into two parts. Part one: a comparative energy and exergy efficiency study of hemispherical solar still and a single-slope solar still. The overall daily productivity was improved by 47.96% for the hemispherical solar still compared to the single-slope solar still. The maximum daily energy efficiency and exergy efficiency of the single-slope solar still are 25.81 and 1.8%, respectively, and for hemispherical solar still are 38.61 and 3.1%, respectively. The main conclusion from the study is the hemispherical distillery greatly enhances productivity as compared to the single slope distillate and gives more efficiency. Thus, the hemispherical solar still is recommended to be used to provide safe drinking water from salty water.

Part two: The hemispherical distiller characteristics are having a large surface area for receiving and condensing compared to a conventional single-slope distiller. To achieve the maximum possible utilization of this feature, in first the $Al_2O_3$ nanoparticles were adding to the basin water to increase the evaporation rate, in the second modification the glass cover cooling technology was utilized to increase the condensation rate. To investigate the influences of $Al_2O_3$-water nanofluid and the glass cover cooling technology by a water sprinkler on hemispherical solar distiller performance, three hemispherical solar distillers were designed and tested in the same climate conditions. The first is the reference case (conventional hemispherical solar distiller), second is the modified hemispherical solar distiller with $Al_2O_3$-water nanofluid, and the third is the modified hemispherical solar distiller with $Al_2O_3$-water nanofluid and water sprinkler. Three different concentrations of $Al_2O_3$ nanoparticles 0.1, 0.2, and 0.3% were studied. Results showed that, the improvement 41.8, 50.9, and 61.3% of the volume friction of 0.1, 0.2, and 0.3%, respectively. Also, the improvement for utilizing the $Al_2O_3$ nanoparticles and water sprinkler reached 105.8, 110.4, and 121% for nanoparticle concentrations 0.1, 0.2, and 0.3%, respectively as compared to the reference case.

**Keywords**: Solar energy; Nano- $Al_2O_3$; Hemispherical solar distiller; Single-slope solar distiller; Water sprinkler; Constant water flow rate; Distilled water; Productivity.

**الملخص:** تنقسم هذه الأطروحة إلى قسمين. القسم الأول: دراسة مقارنة للطاقة وكفاءة الطاقة للمقطرات الشمسية نصف الكروية وأحادية المنحدر. تم تحسين الإنتاجية اليومية الإجمالية بنسبة 47.96 ٪ للمقطرات الشمسية نصف الكروية مقارنةً بالمقطرات الشمسية أحادية المنحدر. الحد الأقصى لكفاءة الطاقة اليومية وكفاءة الطاقة للمقطرات الشمسية أحادية المنحدر هي 25.81 و 1.8٪ على التوالي، وبالنسبة للمقطرات الشمسية نصف الكروية 38.61 و 3.1٪ على التوالي. الاستنتاج الرئيسي من الدراسة هو أن جهاز التقطير النصف كروي يعزز الإنتاجية بشكل كبير بالمقارنة مع نواتج التقطير أحادية المنحدر ويعطي المزيد من الكفاءة. وبالتالي، يوصى باستخدام جهاز التقطير الشمسي النصف كروي لتوفير مياه شرب آمنة من المياه المالحة.

الجزء الثاني: تتميز خصائص جهاز التقطير نصف الكروي بمساحة كبيرة للاستقبال والتكثيف مقارنة بجهاز التقطير الشمسي أحادية المنحدر. لتحقيق أقصى استفادة ممكنة من هذه الميزة ، في البداية تم إضافة جزيئات $Al_2O_3$ النانوية إلى ماء الحوض لزيادة معدل التبخر، وفي التعديل الثاني تم استخدام تقنية تبريد الغطاء الزجاجي لزيادة معدل التكثيف. للتحقيق في تأثيرات السائل النانوي المائي $Al_2O_3$ وتقنية تبريد الغطاء الزجاجي بواسطة رشاش ماء على أداء جهاز التقطير الشمسي نصف كروي، تم تصميم واختبار ثلاثة مقطرات شمسية نصف كروية في نفس الظروف المناخية. الأول هو الحالة المرجعية (المقطر الشمسي التقليدي)، والثاني هو المقطر الشمسي نصف كروي المعدل باستخدام مائع نانوي الماء $Al_2O_3$ ، والثالث هو المقطر الشمسي نصف كروي المعدل باستخدام سائل نانوي ماء $Al_2O_3$ مع تبريد الغطاء. تمت دراسة ثلاثة تراكيز مختلفة من جزيئات $Al_2O_3$ النانوية 0.1 و 0.2 و 0.3٪. أظهرت النتائج أن نسبة التحسن هي 41.8 و 50.9 و 61.3٪ عند استخدام جزيئات $Al_2O_3$ النانوية بالتراكيز 0.1 و 0.2 و 0.3٪ على التوالي. كما بلغ التحسن 105.8 و 110.4 و 121٪ عند استخدام تركيزات الجسيمات النانوية 0.1 و 0.2 و 0.3٪ على التوالي، مع تبريد الغطاء، مقارنة بالحالة المرجعية.

**الكلمات المفتاحية:** الطاقة الشمسية؛ نانو-$Al_2O_3$؛ المقطر الشمسي النصف كروي؛ المقطر الشمسي أحادي المنحدر؛ تبريد الغطاء الزجاجي؛ معدل تدفق المياه ثابت؛ الماء المقطر؛ الإنتاجية.